Dynamic harmonization of source-oriented and receptor models for source apportionment

Science of the Total Environment 859 (2023) 160312

Contents lists available at ScienceDirect

Science of the Total Environment

journal homepage: www.elsevier.com/locate/scitotenv

Dynamic harmonization of source-oriented and receptor models for source apportionment

Xiaole Zhang [a,b,d,1], Xiaoxiao Feng [a,b,1], Jie Tian [c,1], Yong Zhang [c], Zhiyu Li [c], Qiyuan Wang [c], Junji Cao [c], Jing Wang [a,b,*]

[a] Institute of Environmental Engineering (IfU), ETH Zürich, Zürich CH-8093, Switzerland
[b] Laboratory for Advanced Analytical Technologies, Empa, Dübendorf CH-8600, Switzerland
[c] Key Laboratory of Aerosol Chemistry and Physics, State Key Laboratory of Loess and Quaternary Geology, Institute of Earth Environment, Chinese Academy of Sciences, Xi'an, China
[d] Institute of Public Safety Research, Department of Engineering Physics, Tsinghua University, Beijing, China

HIGHLIGHTS

- Source-oriented and receptor models for source apportionment are dynamically harmonized.
- Primary $PM_{2.5}$ emissions from key sectors are updated based on Bayesian Inference.
- Primary $PM_{2.5}$ from the local sources in Beijing has significantly declined from 2017 to 2021.
- Regional transport becomes a dominant contributor to the primary $PM_{2.5}$ in Beijing in 2021.

GRAPHICAL ABSTRACT

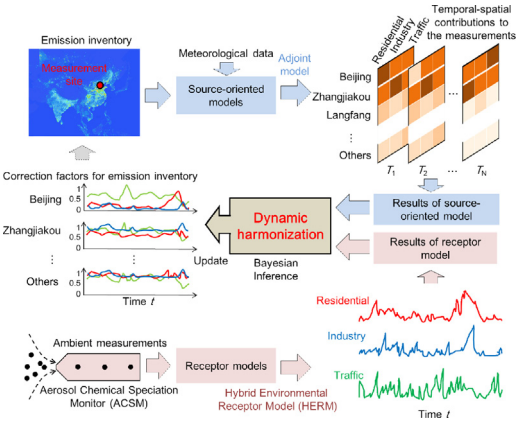

ARTICLE INFO

Editor: Hai Guo

Keywords:
Source apportionment
Source-oriented model
Receptor model
Bayesian inference
Emission inventory

ABSTRACT

Millions of premature mortalities are caused by the air pollution of fine particulate matter with aerodynamic diameters less than 2.5 μm ($PM_{2.5}$) globally per year. To effectively control the dominant emission sources and abate air pollution, source apportionment of $PM_{2.5}$ is normally conducted to quantify the contributions of various sources, but the results of different methods might be inconsistent. In this study, we dynamically harmonized the results from the two dominant source apportionment methods, the source-oriented and receptor models, by updating the emission inventories of primary $PM_{2.5}$ from the major sectors based on the Bayesian Inference. An adjoint model was developed to efficiently construct the source-receptor sensitivity matrix, which was the critical information for the updates, and depicted the response of measurements to the changes in the emissions of various sources in different regions. The harmonized method was applied to a measurement campaign in Beijing from January to February 2021. The results suggested a significant reduction of primary $PM_{2.5}$ emissions in Beijing. Compared with the baseline emission inventory of 2017, the primary $PM_{2.5}$ emissions from the local residential combustion and industry in Beijing had significantly declined by about 90 % during the investigated period of the year, and the traffic emission decreased by about 50 %. The proposed methods successfully identified the temporally dynamic changes in the emissions induced by the Spring Festival. The methods could be a promising pathway for the harmonization of source-oriented and receptor source apportionment models.

* Corresponding author at: Institute of Environmental Engineering (IfU), ETH Zürich, Zürich CH-8093, Switzerland.
E-mail address: jing.wang@ifu.baug.ethz.ch (J. Wang).
[1] These authors contributed equally to this work.

http://dx.doi.org/10.1016/j.scitotenv.2022.160312
Received 27 August 2022; Received in revised form 15 November 2022; Accepted 15 November 2022
Available online xxxx

1. Introduction

Exposure to ambient fine particulate matter with diameters less than 2.5 μm ($PM_{2.5}$) causes millions of premature mortalities annually, which is recognized as a leading global health concern (Forouzanfar et al., 2016; Lelieveld et al., 2015). The information about source-specific contributions to ambient $PM_{2.5}$ is of great importance for implementing effective measures to control and abate air pollution (Karagulian et al., 2015; Laupsa et al., 2009; Viana et al., 2008). Source apportionment techniques are widely applied to quantify the contributions of various sources to ambient air pollution (Chen Antony and Cao, 2018; Huang et al., 2014; Viana et al., 2008).

Accurate source apportionment of $PM_{2.5}$ is still challenging and complex. The receptor model and source-oriented model are the two dominant methods for source apportionment (Viana et al., 2008; Zhu et al., 2018). The receptor models are based on mass balance analysis and statistical evaluation of chemical data of particulate matter acquired at receptor sites to re-construct the contributions from different types of sources (Hopke et al., 2006). The receptor models usually assume that there is no significant change in the profiles of chemical compositions of sources during transport from sources to receptors, and no chemical reaction or phase partitioning in the receptor species (Belis et al., 2013). The commonly utilized receptor models include Chemical Mass Balance (CMB) (Henry et al., 1984; Watson et al., 1984), Principal Component Analysis (PCA) (Thurston and Spengler, 1985; Viana et al., 2006), and Positive Matrix Factorization (PMF) (Paatero and Tapper, 1994; Reff et al., 2007). Refined comprehensive receptor models rely on high-end measurement instruments, which have relatively low uncertainties, but the number of measurement sites is usually limited. The results of receptor models might suffer from the representativeness of the measurement sites and face challenges to distinguish the spatial contributions from different regions.

Source-oriented models utilize emission inventories and atmospheric transport models to evaluate the contributions of different types of sources (Chen et al., 2017; Gao et al., 2022; Kelly et al., 2016; Laupsa and Slordal, 2003; Snoun et al., 2019; Ying et al., 2018; Zhang et al., 2018; Zhang et al., 2021; Zhang et al., 2020; Zhang and Wang, 2021). Different approaches have been developed to distinguish the impacts of various sources in the atmospheric models, including the Particulate Matter Source Apportionment Technology (PSAT) (Wagstrom et al., 2008) in the Comprehensive Air quality Model with extensions (CAMx) (Gaydos et al., 2007), Tagged Species Source Apportionment (TSSA) (Wang et al., 2009) in the Community Multiscale Air Quality Model (CMAQ), the Integrated Source Apportionment Method (ISAM) (Kwok et al., 2013) in CMAQ, the CMAQ decoupled direct method (CMAQ-DDM) (Hu et al., 2009), and the adjoint model of CMAQ (Zhao et al., 2020) and GEOS-Chem (Henze et al., 2009) for source-receptor sensitivity analysis. Source-oriented models are normally less resource-demanding than receptor models and can achieve high spatial and temporal resolutions. The source-oriented models are based on the emission inventories, which could better represent the regional contributions than the receptor models, but a large amount of survey data should be collected for compiling emission inventories (Li et al., 2017a; Zhang et al., 2022b; Zhang et al., 2019; Zheng et al., 2018) and they are easy to be outdated, causing large uncertainties.

The receptor models and source-oriented models are generally applied independently. The results of the two methods might be inconsistent, but they are mutually complementary. By harmonizing the two methods, the emission inventory in the source-oriented model can be dynamically updated by the high-quality measurements of the receptor model, and the source-oriented model using the updated emission inventory is able to quantify the regional contributions and alleviate the representative problem of sampling in the receptor model. The recent technical report of the Joint Research Centre of the European Commission has suggested the combination and harmonization of the two approaches (Mircea et al., 2020), and some attempts have been made in this direction. The PMF receptor model was combined with the source-oriented AirQUIS-EPISODE model to constrain the local emissions from different sectors in Oslo, Norway (Laupsa et al., 2009). The source-oriented model using CMAQ with brute-force method (BFM) has been compared with the PMF receptor model to identify the bias in the emission data in Japan, but the emissions were not updated (Uranishi et al., 2017). The source apportionment of precursors (SO_2, NOx, VOCs, NH_3) by the CAMx-PSAT or CMAQ source-oriented models were utilized to approximate the source contributions to secondary $PM_{2.5}$, which were directly added to the results of receptor models for primary $PM_{2.5}$ to evaluate the source contributions to atmospheric $PM_{2.5}$ (Lang et al., 2017a; Lang et al., 2017b). A hybrid source apportionment method has been developed using detailed species measurements of $PM_{2.5}$ and the chemical mass balance method to update the results of the CMAQ-DDM source-oriented model, but emission inventories were not updated (Hu et al., 2014; Ivey et al., 2015). Most of the previous studies utilized offline source apportionment with long sampling periods and low temporal resolution, so it was difficult for them to dynamically update or identify the rapidly changing emissions. It was usually computationally expensive to calculate the source-specific response of measurements to the emissions in multiple regions using the existing source-oriented models, e.g. CMAQ-DDM. Due to the above limitation, local emissions were updated without consideration of regional transport (Laupsa et al., 2009), or spatial corrections were achieved by spatial interpolation of the local results at multiple sites (Hu et al., 2014; Ivey et al., 2015). In general, the development of methods for harmonization of receptor models and source-oriented models is still in its infancy.

In this study, we aimed to dynamically update the emission inventories of primary $PM_{2.5}$ from the major sectors by the combination of the source-oriented model and the online receptor source apportionment model with a high temporal resolution based on the Bayesian Inference. The hourly receptor source apportionment results were obtained using the Hybrid Environmental Receptor Model (HERM) (Chen Antony and Cao, 2018) with the measurements collected by online instruments. We developed an adjoint atmospheric transport model to efficiently construct the source-receptor sensitivity matrix, which depicted the response of the measurements to the changes in the emission sources in 33 regions. The temporally dynamic update with the high temporal resolution was achieved by using the rolling-window Bayesian Inference with source-receptor sensitivity matrix, the baseline emission inventory for 2017, and the results of the receptor model. The combined method was applied to a measurement campaign in Beijing from January to February 2021. The emissions of three types of sources, i.e. residential combustion, traffic, and industry, were hourly updated considering both the local and regional transport from the 33 regions in the computational domain, and the impacts of the Spring Festival on the emissions were successfully identified. The methods proposed in the study could be a promising pathway for achieving timely updated emission inventories and harmonizing the source-oriented and receptor source apportionment models.

2. Data and methods

2.1. Emission inventories

Atmospheric model and emission inventories were utilized to evaluate the primary $PM_{2.5}$ concentrations (Hu et al., 2015; Karl et al., 2022; Zhang et al., 2022a; Zhang and Wang, 2022). We combined three emission inventories to generate the final emission data covering the whole investigated domain: the Beijing-Tianjin-Hebei (BTH) emission inventory (Zheng et al., 2021; Zheng et al., 2017), the mosaic Asian anthropogenic emission inventory (MIX) (Li et al., 2017b), and the Multi-resolution Emission Inventory for China (MEIC) Version 1.3 (Li et al., 2017a; Zheng et al., 2018). The high resolution (0.1 by 0.1°) emission inventory BTH for 2017 was applied in Beijing, Tianjin, and Hebei, closely surrounding the measurement site in Beijing. The emission inventory of MEIC for 2017 with a spatial resolution of 0.25° was adopted for other regions in China. The MIX emission inventory for 2010 with a spatial resolution of 0.25° was utilized for other Asian areas. The new high-resolution temporal profiles (Crippa et al., 2020) from the Emission Database for Global

Atmospheric Research (EDGAR) Version 5.0 (Crippa et al., 2019) were applied to the emission inventories.

2.2. Atmospheric transport model

The atmospheric transport of the primary $PM_{2.5}$ from different sources was calculated by the Eulerian chemistry-transport model POLAIR 3D (version 1.10) in the POLYPHEMUS platform (Mallet et al., 2007). We have evaluated the model by successfully reproducing the dispersion processes in the first European Tracer Experiment (ETEX) (Zhang et al., 2015a) and the Kincaid power plant tracer experiment (Zhang et al., 2015b).

In the current study, the horizontal resolution of the model was 0.1 × 0.1°, with the longitude from 105°E to127°E and the latitude from 30°N to 50°N. The configurations of the model were similar to our previous study in Beijing with the same model (Gao et al., 2022). The 5th generation reanalysis product (ERA5) of the European Center for Medium-Range Weather Forecasts (ECMWF) was adopted as the meteorological data for the model. The ERA5 dataset had a temporal resolution of 1 h and a horizontal resolution of 0.25 × 0.25°. The meteorological data were linearly interpolated onto the grid of the air quality model. The spatial resolution of the dispersion model (0.1°) was close to the resolution of the metrological data (0.25°), so it is reasonable to linearly interpolate the data, which is also the standard preprocessing procedure in the POLAIR 3D model for the reanalysis meteorological data from ECMWF. For a finer resolution, e.g. 0.01°, the meteorological data should be considered to be dynamically downscaled using a mesoscale numerical weather prediction model, e.g. Weather Research and Forecasting (WRF) (Skamarock et al., 2019). There were 11 vertical levels from the surface to 4000 m altitude, which included the boundary layer with significant mixing. The time step was 5 min.

The vertical diffusion coefficients within the boundary layer were estimated by the Troen & Mahrt parameterization model (Troen and Mahrt, 1986), and the Louis parametrization (Louis, 1979) was adopted for other regions. The wet scavenging rates were estimated by the parameterization model proposed by Andronache (Andronache, 2003) based on the precipitation intensity. The dry deposition velocities were estimated by the formula proposed by Venkatram and Pleim (Venkatram and Pleim, 1999; Zhang et al., 2018).

2.3. Adjoint model

The adjoint POLAIR 3D model was developed to efficiently generate the source-receptor sensitivity matrix. The adjoint model has been discussed in detail by Kalnay (Kalnay, 2003). Here we briefly introduce the essential concepts of the adjoint model using the discrete form. The system of atmospheric transport of pollutants can be described as

$$\mathbf{c}(t_N) = M(\boldsymbol{\sigma}(t_0)), \tag{1}$$

where $\mathbf{c}(t_N)$ is the vector of the concentrations at time t_N due to the vector of the emissions of all the grid cells at time t_0, $\boldsymbol{\sigma}(t_0)$, and N is the number of time steps. Namely

$$\mathbf{c}(t_N) = (c_1(t_N), c_2(t_N), \cdots, c_{I\times J\times K}(t_N))^{\mathrm{T}}, \tag{2}$$

$$\boldsymbol{\sigma}(t_0) = (\sigma_1(t_0), \sigma_2(t_0), \cdots, \sigma_{I\times J}(t_0))^{\mathrm{T}}, \tag{3}$$

where I, J, and K are the number of grid cells in the x, y, and z directions of the model. Only the anthropogenic emissions on the ground, namely at the bottom layer of the model, were considered, so the length of the emission vector was $I \times J$. The emissions were injected into the bottom layer in the model, and stack heights or plume rises were not considered. The measurement site was a representative site, which was far from the major sources, e.g. the industrial emissions, so the emitted pollutants from the sources had been vertically well mixed within the atmospheric boundary layer. As a result, the simplifications are reasonable for the measurements in the current study. To compare with the results of receptor models, only the primary $PM_{2.5}$ was calculated by the atmospheric transport model, without complicated chemical reactions, so the model M can be simplified into a linear model, which is represented by the source-receptor sensitivity matrix $\mathbf{M}$, and can be further expressed as the product of consecutive transport matrixes.

$$\mathbf{c}(t_N) = \mathbf{M}\cdot\boldsymbol{\sigma}(t_0) = \mathbf{M}_{t_N}\cdot\mathbf{M}_{t_{N-1}}\cdots\mathbf{M}_{t_0}\cdot\boldsymbol{\sigma}(t_0) \tag{4}$$

The model utilizes the emissions at each grid to generate the source-receptor sensitivity matrix column by column as follows

$$\begin{aligned}\mathbf{c}(t_N) &= \mathbf{M}\cdot(\sigma_1(t_0), \sigma_2(t_0), \cdots, \sigma_{I\times J}(t_0))^{\mathrm{T}}\\ &= \mathbf{M}\cdot(\sigma_1(t_0), 0, \cdots, 0)^{\mathrm{T}} + \mathbf{M}\cdot(0, \sigma_2(t_0), \cdots, 0)^{\mathrm{T}} + \cdots + \mathbf{M}\\ &\quad\cdot(0, 0, \cdots, \sigma_{I\times J}(t_0))^{\mathrm{T}}\end{aligned} \tag{5}$$

As a result, the atmospheric model has to be run for $I \times J$ times to obtain each column of the matrix $\mathbf{M}$, which is too computationally expensive. The matrix $\mathbf{M}$ contains the full information of source-receptor sensitivity, but we only need the information for the locations with measurements. Assuming that there is only one measurement site located at grid L, we just need to obtain the entries of the source-receptor sensitivity matrix between all the sources and the concentration at grid L. We multiply Eq. (4) with a vector, which has 1 at the L position and 0 at the other positions,

$$(0, \cdots 1 \cdots, 0)\cdot\mathbf{c}(t_N) = (0, \cdots 1 \cdots, 0)\cdot\mathbf{M}_{t_N}\cdot\mathbf{M}_{t_{N-1}}\cdots\mathbf{M}_{t_0}\cdot\boldsymbol{\sigma}(t_0). \tag{6}$$

The concentration at grid L becomes

$$c_L(t_N) = \left(\mathbf{M}_{t_0}{}^{\mathrm{T}}\cdots\cdot\mathbf{M}_{t_{N-1}}{}^{\mathrm{T}}\cdot\mathbf{M}_{t_N}{}^{\mathrm{T}}\cdot(0, \cdots 1 \cdots, 0)^{\mathrm{T}}\right)^{\mathrm{T}}\cdot\boldsymbol{\sigma}(t_0). \tag{7}$$

The adjoint model can be defined as

$$\widehat{\mathbf{c}}(t_N) = \mathbf{M}_{t_0}{}^{\mathrm{T}}\cdots\cdot\mathbf{M}_{t_{N-1}}{}^{\mathrm{T}}\cdot\mathbf{M}_{t_N}{}^{\mathrm{T}}\cdot(0, \cdots 1 \cdots, 0)^{\mathrm{T}}. \tag{8}$$

The adjoint model is equivalent to the atmospheric model with a unit emission at the grid L, but backward in time and with the transpose of the transport matrix. The transpose of the advection term means the reverse wind directions, manifested by the linear upstream advection scheme. The diffusion and deposition terms are symmetric, namely self-adjoint. The adjoint model has been developed according to Eq. (8), which only needs to run the atmospheric transport model once to obtain the contributions of all the sources to the measurements at grid L,

$$\begin{aligned}c_L(t_N) &= \widehat{\mathbf{c}}(t_N)^{\mathrm{T}}\cdot\boldsymbol{\sigma}(t_0)\\ &= \widehat{\mathbf{c}}(t_N)^{\mathrm{T}}\cdot(\sigma_1(t_0), 0, \cdots, 0)^{\mathrm{T}} + \widehat{\mathbf{c}}(t_N)^{\mathrm{T}}\cdot(0, \sigma_2(t_0), \cdots, 0)^{\mathrm{T}} + \cdots\\ &\quad + \widehat{\mathbf{c}}(t_N)^{\mathrm{T}}\cdot(0, 0, \cdots, \sigma_{I\times J}(t_0))^{\mathrm{T}}.\end{aligned} \tag{9}$$

In the study, the adjoint model was run backward for 240 h (10 days) for each measurement time. The point t_0 indicated a given time between 1 and 240 h before the measurement. The adjoint model runs only once backwardly up to 240 h before the measurement and saves all the hourly intermediate results. Each hourly intermediate result contains the contributions of the emissions released at that point in time by all sources to the measurement. As a result, the source-receptor sensitivity matrix for each measurement contains the hourly contributions from all the sources up to 10 days before the measurement. The backward period (10 days) was long enough to include almost all the contributions to the measurements, as evidenced by the good agreement between the direct results and adjoint results, which are discussed in Section 3.1.

2.4. Receptor model

The results of the atmospheric transport model were compared with the results of the receptor model, which also identified the primary contributions of different sources. The hourly measurement of $PM_{2.5}$ was conducted between January 17 and February 20, 2021 at the observation site

(116.39° E, 39.98° N) of the Institute of Atmospheric Physics, Chinese Academy of Sciences, Beijing. The compositions of $PM_{2.5}$ were measured with Quadrupole Aerosol Chemical Speciation Monitor (Q-ACSM, Aerodyne Research Inc., Billerica, Massachusetts, USA), Xact 625i Ambient Metals Monitor (X625i, Cooper Environmental Services, Beaverton, OR, USA) and Aethalometer (Model AE33, Magee Scientific, Berkeley, CA, USA). The Q-ACSM measured NO_3^-, SO_4^{2-}, NH_4^+, Cl^-, and organic aerosol (OA) compositions in $PM_{2.5}$. The X625i monitored the inorganic elements, including Si, K, Ca, Cr, Mn, Fe, Ni, Cu, Zu, As, Se, Ba, and Pb. The Model AE33 measured the black carbon composition. Fig. S1 in the Supporting Information (SI) shows the composition of $PM_{2.5}$ in Beijing during the sampling period, which was mainly composed of OA (36.3 %), followed by NO_3^- (25.1 %), SO_4^{2-} (15.9 %), NH_4^+ (15.2 %), inorganic elements (3.2 %), BC (3.1 %), and Cl^- (1.2 %). More information about the monitoring instruments could be found in our previous studies (Tian et al., 2021a; Tian et al., 2021b).

The Hybrid Environment Receptor Model (HERM) was utilized for the source apportionment of $PM_{2.5}$. The HERM model unifies the effective-variance chemical mass balance (EV-CMB) and positive matrix factorization (PMF) models (Chen Antony and Cao, 2018). The source profile and the corresponding contributions were obtained by iteratively minimizing the objective function Q, which was defined as

$$Q = \Sigma_{j=1}^{N_{composition}} \Sigma_{i=1}^{N_{sample}} \frac{\left(x_{ij} - \Sigma_{k=1}^{N_{source}} g_{ik} f_{kj}\right)^2}{\sigma_{x_{ij}}^2 + \Sigma_{k=1}^{N_{source}} \left(g_{ik}^2 \sigma_{f_{kj}}^2 + \delta_{ik} \sigma_{x_{ij}}^2\right)} \tag{10}$$

where N_{sample}, $N_{composition}$, and N_{source} respectively denote the total numbers of samples, chemical compositions and the target sources, x_{ij} is the matrix of the measured chemical compositions of $PM_{2.5}$, f_{kj} is the matrix of the source profiles, g_{ik} is the matrix of contributions from the sources, $\sigma_{x_{ij}}$ and $\sigma_{f_{kj}}$ are respectively the uncertainties in the measured chemical compositions and the source profiles, and g_{ik} and f_{kj} are unknowns and to be solved. δ_{ik} is set as 0 when the profile of the kth source is fixed and considered as known and set as 1 when the profile will be estimated. Based on the HERM model and online measurements of $PM_{2.5}$, eight sources were identified by the explained variation in chemical species, including biomass burning, coal combustion, industrial emission, traffic emission, dust, firework, secondary nitrate, and secondary sulfate (Section S1 and Fig. S2 in SI). A detailed description of the source identification can be found in our paper focused on source apportionment (Zhang et al., 2022c) (submitted for publication).

2.5. Matching categories of emission sources

We first harmonized the source categories of the receptor model and the source-oriented model to facilitate the comparison between them. Five types of primary anthropogenic sources of $PM_{2.5}$ were identified in the receptor model, i.e. biomass burning, coal combustion, industrial emission, traffic emission, and firework. Firework emissions mainly happened during the Spring Festival, and it was challenging to identify the sources spatially. The contribution of fireworks was only about 4 % of the total primary $PM_{2.5}$ concentrations, so the firework emissions were not included in the harmonization.

In the source-oriented model, all of the three adopted emission inventories (BTH, MIX, and MEIC) reported the emissions of the three major categories of anthropogenic sources, i.e. residential combustion, traffic, and industry, which are the dominant contributors to $PM_{2.5}$ in Beijing in the winter heating period (Chang et al., 2019). The three categories of sources in the source-oriented model are corresponding to the four types of sources in the receptor model. Our goal was to update the emission inventories, so the source types in the emission inventories were kept, and the contributions of the four types of sources in the receptor model were allocated into the three categories of the source-oriented model. The primary $PM_{2.5}$ used in this study refers to $PM_{2.5}$ from biomass burning, coal combustion, industrial emission, and traffic emission.

The contribution of biomass burning was completely assigned to residential combustion. Coal combustion was caused by both residential and industrial sources. Two assumptions were introduced to allocate the coal combustion. First, it was assumed that the portion of coal combustion attributable to industrial sources was correlated with industrial emissions identified by the receptor model, and they had the same temporal fluctuation. Second, it was assumed that the average ratio between the primary $PM_{2.5}$ emissions from residential coal combustion and biomass burning was about 1:2 after 2015, as estimated by the survey of solid fuel consumption for the residential sector in China (Peng et al., 2019). As a result, the portions of coal combustion attributable to industrial sources $C_{\mathrm{coalToInd}}$ and to residential sources $C_{\mathrm{coalToResid}}$ were estimated as

$$c_{\mathrm{coalToInd}}(t) = \frac{\overline{c_{\mathrm{coal}}(t)} - 0.5 \cdot \overline{c_{\mathrm{bioBurn}}(t)}}{\overline{c_{\mathrm{industry}}(t)}} \cdot c_{\mathrm{industry}}(t) \tag{11}$$

$$c_{\mathrm{coalToResid}}(t) = c_{\mathrm{coal}}(t) - c_{\mathrm{coalToInd}}(t) \tag{12}$$

where $c_{\mathrm{coal}}(t)$, $c_{\mathrm{bioBurn}}(t)$ and $c_{\mathrm{industry}}(t)$ were the temporal contributions from coal combustion, biomass burning, and industrial emissions identified by the receptor model. $\overline{c(t)}$ was the time average of the contributions. The relation was identified in the recent nationwide field survey in China, especially in the North China Plain (Peng et al., 2019), which is the region with the strongest influence in this study. According to the relation, most of the coal combustion was attributed to residential combustion, which was considered to be reasonable due to the much higher emission factors of residential coal combustion than those of industry (Li et al., 2017a). It might underestimate the overall contributions of the industry, which is better to be further investigated with more available information. As a result, the final contribution of the residential sector was $c_{\mathrm{coaltoRes}} + c_{\mathrm{bioburn}}$ and the final contribution of the industry was $c_{\mathrm{industry}} + c_{\mathrm{coaltoind}}$.

2.6. Dynamic updates of emission inventory

The whole computational domain was divided into 33 regions, including Beijing, 11 cities in Hebei Province, 20 regions at the province level in China, and the other regions as a whole in the computational domain. The locations of the regions are shown in Fig. S3 in SI. The emissions in Beijing and Hebei were updated at the city level since they directly flanked the measurement site in Beijing and had a significant influence on the measurements. The emissions were updated at the province level for other regions, which were far from the measurement site. The emissions of the three major types of sources, i.e. residential combustion, traffic, and industry, were dynamically updated for the 33 regions by the harmonization of source-oriented and receptor models based on the Bayesian Inference, which has been successfully applied to estimate emissions from accidental releases (Cai et al., 2022; Wang et al., 2018; Wu et al., 2018; Wu et al., 2021; Yuan et al., 2019; Zhang et al., 2017; Zhang et al., 2013; Zhang et al., 2014). The spatial distribution of individual types of emissions within each region was not affected by the update, but the magnitude of the emissions was rescaled using a single factor for each region. As a result, 99 (33 regions × 3 categories of sources) rescaling factors were generated in each update.

The dynamic update was achieved by using the rolling-window analysis. The size of the rolling window was 72 h, namely 3 days. As a result, there were 72 consecutive hourly results from the receptor and the source-oriented model within each rolling window, which provided enough data to update the emissions in the 33 regions. The increment between successive rolling windows was 24 h. The Bayesian Inference was applied to update the emissions of the three types of sources in the 33 regions within each rolling window,

$$P(\boldsymbol{\sigma}|\mathbf{c}_{\mathrm{receptor}}) = \frac{P(\mathbf{c}_{\mathrm{receptor}}|\boldsymbol{\sigma})P(\boldsymbol{\sigma})}{P(\mathbf{c}_{\mathrm{receptor}})} \propto P(\mathbf{c}_{\mathrm{receptor}}|\boldsymbol{\sigma})P(\boldsymbol{\sigma}), \tag{13}$$

where $\mathbf{c}_{\mathrm{receptor}}$ was the concentrations induced by a certain type of source within a rolling window, which was estimated by the receptor

model, and $\boldsymbol{\sigma}$ was the emissions of the same type of source in the 33 regions. $P(\boldsymbol{\sigma}|\mathbf{c}_{\text{receptor}})$ is the conditional probability of the emissions given the concentrations attributable to the source estimated by the receptor model. $P(\mathbf{c}_{\text{receptor}}|\boldsymbol{\sigma})$ is the conditional probability of the concentrations given the emissions, and it is usually referred to as the likelihood function. $P(\mathbf{c}_{\text{receptor}}|\boldsymbol{\sigma})$ was evaluated by the differences between the results of the receptor model and the source-oriented model using the emission inventory. As introduced above, the results of the source-oriented model were obtained by the adjoint model to reduce the computational cost as shown in Eq. (9). It is very difficult to identify the actual distribution of errors in the model or the a priori information. As the simplest assumption, the Gaussian type of errors were usually assumed and widely used for the inverse modeling of emissions, and there was usually no significant influence on the quality of results due to the assumption evaluated by tracer experiments (Issartel, 2003; Krysta et al., 2008). In this study, it was also assumed that the likelihood function and the a priori probability followed the normal distribution.

$$P(\mathbf{c}_{\text{receptor}}|\boldsymbol{\sigma}) = \frac{1}{(2\pi)^{N/2}|\mathbf{R}|^{1/2}}\exp\left(-\frac{1}{2}\left(\mathbf{c}_{\text{receptor}} - \hat{\mathbf{c}}^{\mathrm{T}}\cdot\boldsymbol{\sigma}\right)^{\mathrm{T}}\cdot\mathbf{R}^{-1}\cdot\left(\mathbf{c}_{\text{receptor}} - \hat{\mathbf{c}}^{\mathrm{T}}\cdot\boldsymbol{\sigma}\right)\right), \quad (14)$$

where N was the length of the concentration vector $\mathbf{c}_{\text{receptor}}$, and it was 72 for each rolling window. $\mathbf{R}$ was the covariance matrix, which was assumed to be a diagonal matrix with equal diagonal entries, namely,

$$\mathbf{R} = \lambda_{\text{receptor}}\cdot\mathbf{I}_N, \quad (15)$$

where $\mathbf{I}_N$ was the identity matrix of size $N \times N$. $\lambda_{\text{receptor}}$ quantified the magnitude of the uncertainties in the differences between the receptor model and the source-oriented model. The a priori probability $P(\boldsymbol{\sigma})$ of the emission $\boldsymbol{\sigma}$ was also assumed to follow the normal distribution

$$P(\boldsymbol{\sigma}) = \frac{1}{(2\pi)^{M/2}|\mathbf{B}|^{1/2}}\exp\left(-\frac{1}{2}(\boldsymbol{\sigma}-\boldsymbol{\sigma}_0)^{\mathrm{T}}\cdot\mathbf{B}^{-1}\cdot(\boldsymbol{\sigma}-\boldsymbol{\sigma}_0)\right), \quad (16)$$

where M was the number of regions to be updated, and it was 33 as explained above, for each type of source. $\boldsymbol{\sigma}_0$ was the baseline emission from the emission inventory. $\mathbf{B}$ was the covariance matrix to quantify the uncertainties in the emission inventory, which was also assumed to be a diagonal matrix with equal diagonal entries, namely,

$$\mathbf{B} = \lambda_{\text{emission}}\cdot\mathbf{I}_M, \quad (17)$$

where $\lambda_{\text{emission}}$ quantified the magnitude of the uncertainties in the baseline emission inventory. The a posteriori emissions could be expressed as

$$\begin{aligned} P(\boldsymbol{\sigma}|\mathbf{c}_{\text{receptor}}) &\propto P(\mathbf{c}_{\text{receptor}}|\boldsymbol{\sigma})P(\boldsymbol{\sigma}) \\ &= \frac{1}{(2\pi)^{\frac{(N+M)}{2}}|\mathbf{R}|^{\frac{1}{2}}|\mathbf{B}|^{\frac{1}{2}}}\cdot\exp\left(-\frac{1}{2}\left(\left(\mathbf{c}_{\text{receptor}}-\hat{\mathbf{c}}^{\mathrm{T}}\cdot\boldsymbol{\sigma}\right)^{\mathrm{T}}\cdot\mathbf{R}^{-1}\cdot\left(\mathbf{c}_{\text{receptor}}-\hat{\mathbf{c}}^{\mathrm{T}}\cdot\boldsymbol{\sigma}\right)\right.\right. \\ &\quad \left.\left.+(\boldsymbol{\sigma}-\boldsymbol{\sigma}_0)^{\mathrm{T}}\cdot\mathbf{B}^{-1}\cdot(\boldsymbol{\sigma}-\boldsymbol{\sigma}_0)\right)\right), \end{aligned} \quad (18)$$

The optimal emission $\boldsymbol{\sigma}$ was able to maximize the a posteriori probability, which was equivalent to minimizing the following function

$$f(\boldsymbol{\sigma}) = \left(\mathbf{c}_{\text{receptor}} - \hat{\mathbf{c}}^{\mathrm{T}}\cdot\boldsymbol{\sigma}\right)^{\mathrm{T}}\cdot\left(\mathbf{c}_{\text{receptor}} - \hat{\mathbf{c}}^{\mathrm{T}}\cdot\boldsymbol{\sigma}\right) + \frac{\lambda_{\text{receptor}}}{\lambda_{\text{emission}}}(\boldsymbol{\sigma}-\boldsymbol{\sigma}_0)^{\mathrm{T}}\cdot(\boldsymbol{\sigma}-\boldsymbol{\sigma}_0), \quad (19)$$

The matrix $\mathbf{R}$ and $\mathbf{B}$ were replaced with Eqs. (15) and (17). The first term in the equation quantifies the difference between the results of the receptor model and the source-oriented model, and the second term quantifies the deviations of the updated emissions from the original ones. The parameter $\lambda_{\text{receptor}}/\lambda_{\text{emission}}$ was estimated using the L-curve method (Hansen, 2001), which will be introduced in Section 3.2. Eq. (18) was solved by the solver lsqnonneg, for the nonnegative linear least-squares problem, in MATLAB Version R2019b to find the optimized emissions.

A summary of the various uncertainties considered in the current study was shown in Fig. S4. The uncertainties of the source-oriented method contain two major parts, i.e. the uncertainties in the emission inventory and the uncertainties in the atmospheric transport model. The uncertainties in the term of the a priori probability in Eq. (16) contain the uncertainties in the emission inventory. In this study, it was assumed that the uncertainties of the source-oriented model were dominated by the uncertainties in the emission inventory, and the uncertainties induced by the atmospheric transport model were relatively low since the model only calculated the primary emissions and the previous evaluations with the tracer experiments indicated that there was no systematic bias in the model results when accurate emission data were utilized (Zhang et al., 2015a; Zhang et al., 2015b). In the likelihood function in Eq. (14), it is usually hypothesized that the uncertainties are mainly the uncertainties in the observations (Hu et al., 2014). In our study, the covariance matrix $\mathbf{R}$ included both the uncertainties in the receptor model and atmospheric transport. It was assumed that $\mathbf{R}$ was dominated by the uncertainties of the receptor model since the atmospheric transport model had relatively good performance for the primary emissions as evidenced by the tracer experiments.

2.7. Quality indicators for the dynamic updates

The quality of updates for the emission of a target region depends on the contributions of the emission to the concentrations measured at the observation site. The updates for the emission have high quality with strong contributions and low quality with weak contributions. In this study, a quality indicator was adopted to suggest the quality of the updates.

As shown in Fig. S5 in SI, the regional contributions to the concentrations at the measurement site are first sorted in descending order. The top N_H regions, whose contributions as a whole first exceed 90 % of the concentrations at the measurement site, are identified as the major contributors, indicating the emitted pollutants from these regions have reached the measurement site with relatively strong signals. The results are considered as 'high' quality for the N_H regions, indicating high confidence in the results. Then, we identify the top N_M regions, whose accumulative contribution first exceeds 95 %. The results of the regions from $N_H + 1$ to N_M are considered to be of 'medium' quality, suggesting that caution should be exercised about the results. The results of the remaining regions are considered to be of 'low' quality, showing that the results are not reliable.

3. Results

3.1. Quality of the adjoint model

Fig. 1 shows the average spatial distributions of the primary $PM_{2.5}$ attributable to residential combustion, traffic, and industry sources, which were calculated by the atmospheric transport model with the baseline emission inventory for the year 2017 during the measurement period. The contributions from various sources were separated by adding tags to the particulate matter emitted from different sources. The black circle indicated the location of the measurement site. The spatial distribution of the primary $PM_{2.5}$ from residential combustion was relatively homogeneous, with high concentrations in Hebei Province, indicated by the pink boundaries as shown in Fig. 1(a). The primary $PM_{2.5}$ from industry had hot spots with high concentrations, which was due to the industrial point sources.

The concentrations at the measurement site attributable to the three major types of sources were calculated by both the regular atmospheric dispersion model, namely the direct model as shown in Fig. 1, and the adjoint model. The performance of the adjoint model was evaluated by the comparison with the direct model results, as shown in Fig. 2. The adjoint model had a good agreement with the direct model, as evidenced by the distribution along the 1:1 line and by the small average relative error of about 5.2 %. The errors could be caused by the incomplete adjoint forms of the

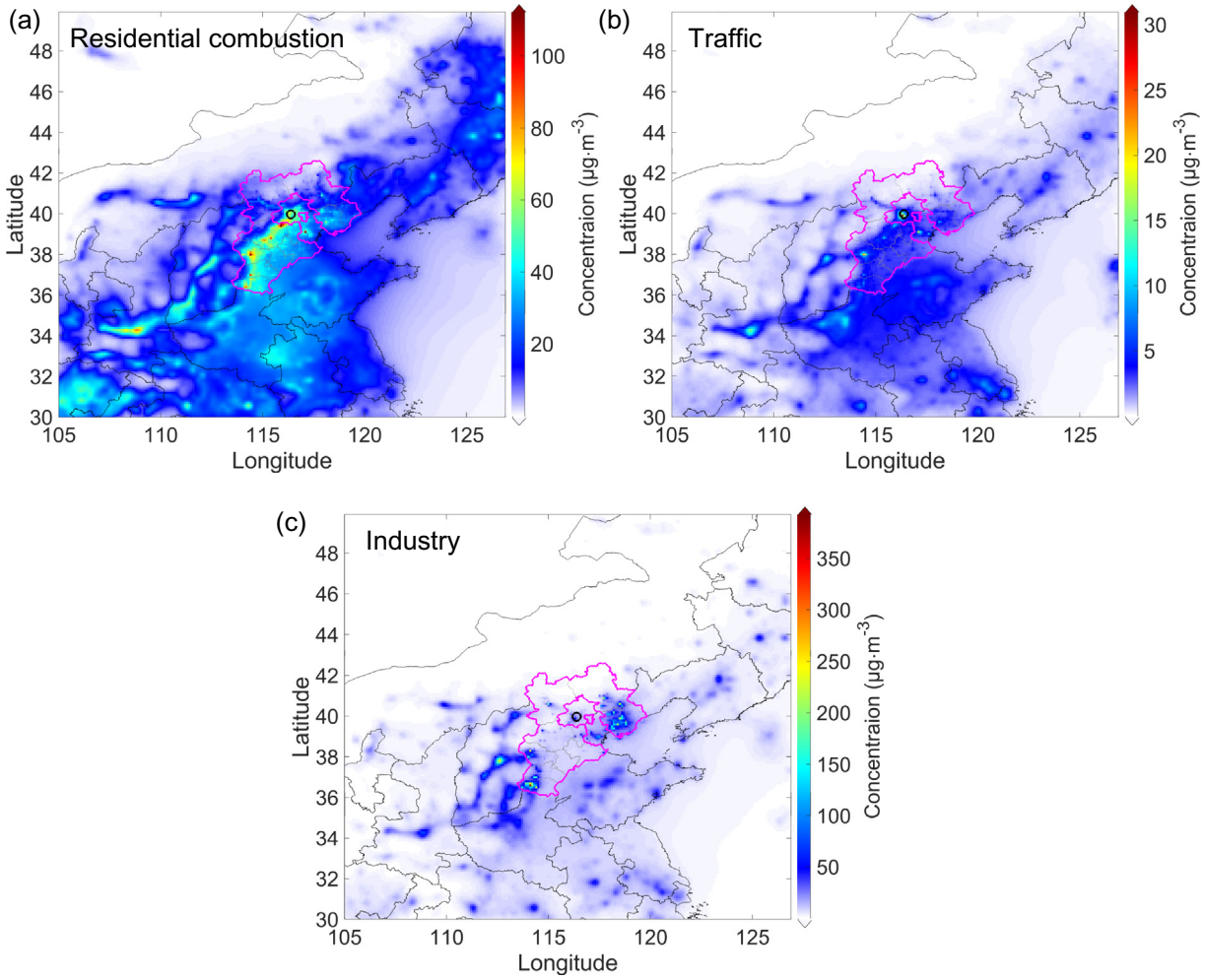

Fig. 1. Average spatial distribution of the primary $PM_{2.5}$ attributable to (a) residential combustion, (b) traffic, and (c) industry sources calculated by the atmospheric transport model with the baseline emission inventory during the measurement period between January 17 and February 20, 2021. The black circle indicated the location of the measurement site. The pink lines marked the boundary of Hebei Province, where the emissions were updated at the city level. The emissions in other regions were updated at the province level.

numerical solvers for advection and diffusion. The errors induced by the adjoint model were considered to be low enough to update the emissions.

3.2. Comparison of primary $PM_{2.5}$ from source-oriented and receptor models

The primary $PM_{2.5}$ concentrations contributed by the residential combustion, industry, and traffic emissions were estimated using the receptor model based on online measurements with a temporal resolution of 1 h. We used the contributions from the three sources as a whole to compare the results of the source-oriented and receptor models to avoid any uncertainties in the apportionment among these sources. Compared with the results of the receptor model, the source-oriented model using the baseline emission inventory for the year 2017 significantly overestimated the total primary $PM_{2.5}$ concentrations from residential combustion, industry, and traffic, during the measurement campaign in 2021, as shown in Fig. 3(a). In order to investigate the similarity of the temporal trends, the concentrations obtained by the source-oriented and receptor models were respectively normalized by the corresponding averages of the whole period. The normalized temporal concentrations had a good agreement with a high correlation coefficient ($r = 0.6$) as shown in Fig. 3(b) and (c). Relatively large differences between the normalized concentrations were observed around February 12, the Spring Festival, when the results of the receptor models were higher than those of the source-oriented model. The differences might be caused by the increases in the emissions, e.g. residential combustion, during the Spring Festival, which was detected by the measurements but failed to be captured in the emission inventory of the source-oriented model.

The results suggested that the dynamically atmospheric transport of the primary $PM_{2.5}$ was well calculated by the source-oriented model, as evidenced by the good agreement of the normalized temporal concentrations, but the baseline emission inventory for 2017 might be outdated for the investigated period in 2021, causing the overestimation of the total primary $PM_{2.5}$. In addition, the temporal changes in emissions due to the Spring Festival were not included in the baseline emission inventory. As a result, it becomes necessary to update the baseline emission inventory by the harmonization of the source-oriented and receptor models.

3.3. Regularization parameters

To update the emission inventory, the L-curve analysis was first utilized to determine the parameter $\lambda_{receptor}/\lambda_{emission}$ in Eq. (19). L-curve is a plot between the 2-norms of the residuals (the differences between the receptor model and the source-oriented model) and the regularized term (the differences between the optimized emissions and the baseline emissions). The L-curve analysis is normally utilized as a graphical tool to investigate the trade-off between the fitting of the data and regularized solution with different regularization parameters (Hansen, 2001; Zhang and Huang, 2017), which are equivalent to the ratios of the uncertainties between $\lambda_{receptor}$ and $\lambda_{emission}$.

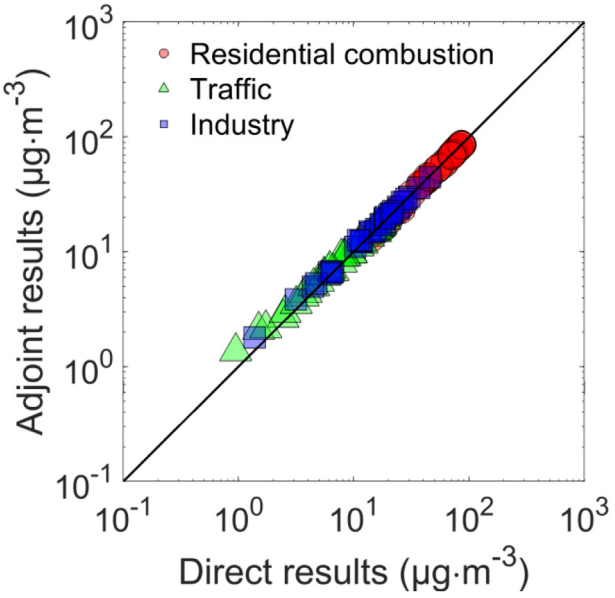

Fig. 2. Comparison between the direct results and the adjoint results (daily average concentrations during the measurement period between January 17 and February 20, 2021).

The L-curve could be split into the horizontal (dashed line) and vertical (solid line) parts, as shown in Fig. 4. The horizontal part had large residuals, indicating that the emissions might be insufficiently updated and the results suffered from potential underfitting. In the vertical part, the residuals were small, but there were significant deviations between the updated and the baseline emissions, which suggested that the emissions could be over-corrected, and the results suffered from potential overfitting. The points at the corner, represented as the blue dots in Fig. 4, simultaneously had low residuals and low deviations from the baseline emissions, which implied a balance between the uncertainties in the likelihood function and the a priori emission inventory. To determine the points at the corner, the curvature of the curve was first calculated. The curvatures of the straight parts were close to zero. The range of the corner was identified when the absolute value of the curvature was larger than the average curvature of the whole curve. The corresponding parameters $\lambda_{receptor}/\lambda_{emission}$ ranged between 30.1 and 90.2 for the points at the corner, which were adopted as the parameters in Eq. (19) to optimize the emissions. The feasible range of $\lambda_{receptor}/\lambda_{emission}$ was utilized to evaluate the uncertainties of the updates.

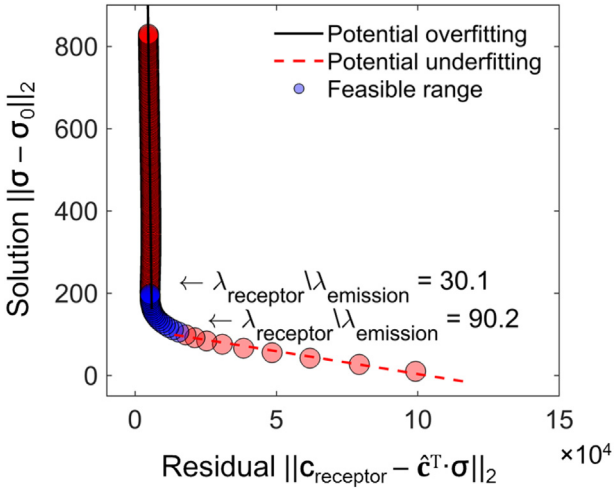

Fig. 4. L-curve between the 2-norms of the residuals (the differences between the receptor model and the source-oriented model) and the regularized term (the differences between the updated emissions and the baseline emissions).

3.4. Dynamic updates of emission

The primary $PM_{2.5}$ emission inventories of the three major types of sources were dynamically updated by the harmonization of the receptor model and the source-oriented model based on the Bayesian Inference. The temporal rescaling factors for the primary $PM_{2.5}$ emissions in Beijing, Langfang (bordering Beijing to the north), and Zhangjiakou (bordering Beijing to the southeast) were shown as examples in Fig. 5. The quality indicators are also shown to indicate the quality of the estimated rescaling factors in Fig. 5. Compared to the baseline emission inventories in 2017, the primary $PM_{2.5}$ emissions from different sectors in Beijing during the period of measurements in 2021 significantly decreased after the updates.

The average rescaling factors for the primary $PM_{2.5}$ emissions of industry and residential combustion in Beijing were respectively about 0.057 and 0.15, which indicated substantial reductions. The quality indicators for the rescaling factors in Beijing were all 'High' as shown in Fig. 5(a), because the observation site was in Beijing and it was always able to detect the local emissions. The reduction could be caused by the three-year action plan to fight air pollution (2018–2020) and the "coal-to-gas" transition in China (Wang et al., 2020), especially for the residential heating in northern China in winters. According to the statistics in the official report of "Beijing Energy Development Plan during the 14th Five-Year Plan Period" (The-People's-Government-of-Beijing-Municipality, 2022), the consumption of

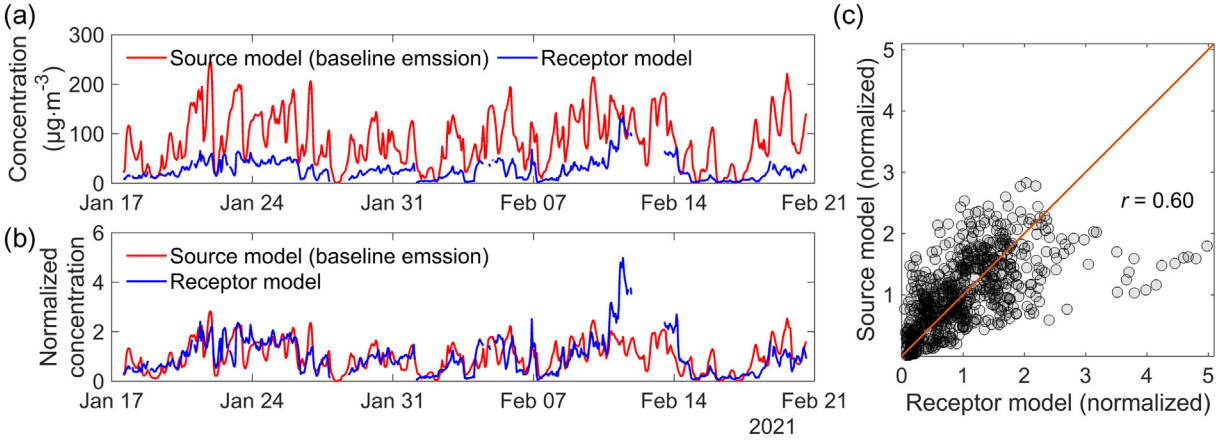

Fig. 3. Comparison of the total primary $PM_{2.5}$ contributed by the residential combustion, industry, and traffic emissions, respectively estimated by the source-oriented and receptor models. (a) Temporal comparison of the concentrations of the total primary $PM_{2.5}$. (b) Temporal comparison of the normalized concentrations of the total primary $PM_{2.5}$. (c) Comparison and correlation between the normalized results of the source model and the receptor model.

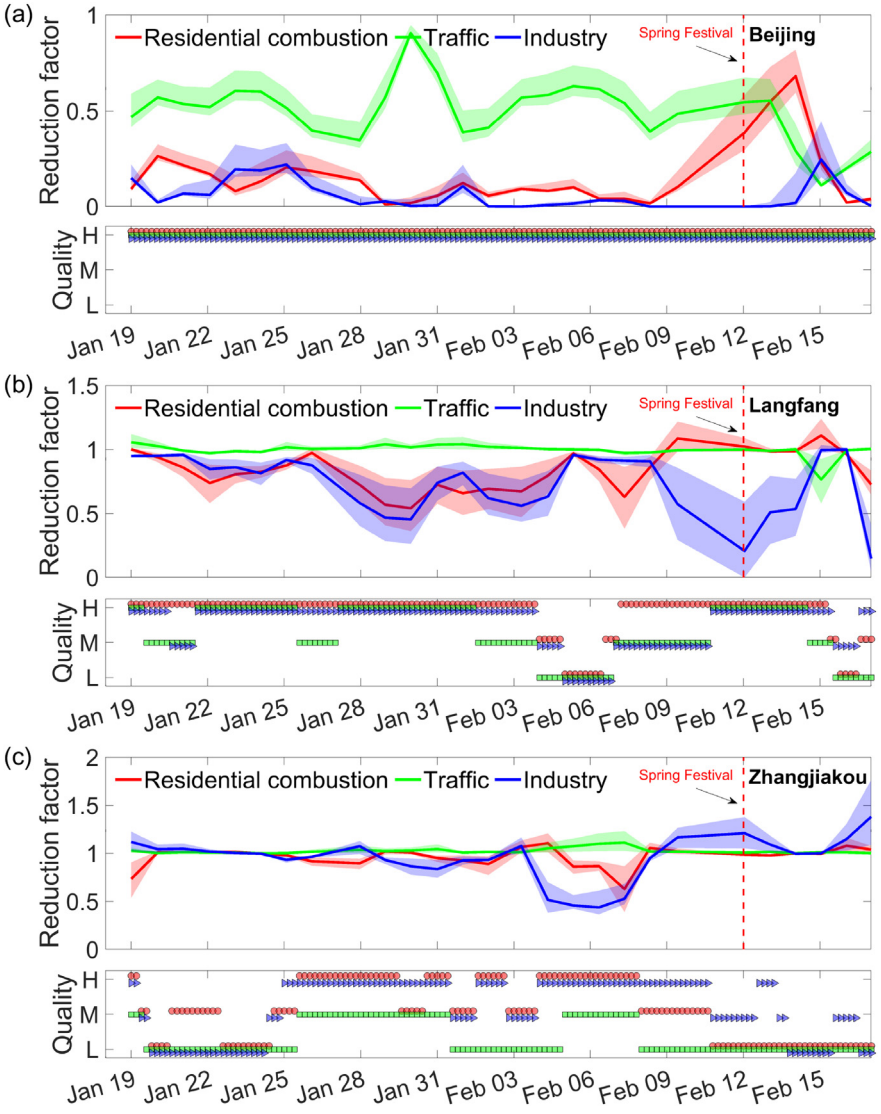

Fig. 5. Temporal rescaling factors for the primary $PM_{2.5}$ emissions in (a) Beijing, (b) Langfang, and (c) Zhangjiakou, from the residential combustion, traffic, and industry sources during the measurement period. The Spring Festival was indicated by the red dashed lines. The shaded area indicated the maximum and minimum values corresponding to the feasible range of $\lambda_{receptor}/\lambda_{emission}$. The quality indicators are also shown for the results, with H for high quality, M for medium quality, and L for low quality.

coal in Beijing was significantly reduced by about 90 % from about 11,652 thousand tons in 2015 to about 1350 thousand tons in 2020. It should be noted that the rescaling factors obtained in the current study only quantified the differences between the emissions during the measurement campaign in January 2021 and the emission inventory for 2017. The rescaling factors might not be accurate enough to quantify the actual emission reduction between 2017 and 2021, considering that the emission inventory might be inaccurate even for the baseline year 2017. The detailed online measurements of $PM_{2.5}$ in 2017 were not available, so it is difficult to evaluate the quality of the baseline emissions using the same methods in the current study. We compared the source model results with the source apportionment studies conducted for January 2014 (Chang et al., 2019) and November/December 2016 (Srivastava et al., 2021), which indicated that the results of the source model in the current study were comparable with the source apportionment results in 2014 and 2016, but they were significantly higher than the harmonization as shown in Fig. S10. The results suggested that the emissions in Beijing have been reduced during the past years, but the quantitative magnitude of reductions needs further investigation.

The reductions in industrial and residential combustion were also observed in Langfang with average rescaling factors of 0.71 and 0.83 respectively. However, the rescaling factors in Langfang within short periods around Feb. 06 and 16 were not reliable with quality indicators of 'Low' as shown in Fig. 5(b). The emissions of residential combustion in Beijing increased during the period of the Spring Festival, which could be caused by the increased energy demand for heating and cooking during the festival, especially in the rural areas of Beijing.

The traffic emissions in Beijing also declined, with an average rescaling factor of 0.49, but the magnitude of the reduction in traffic emissions was smaller compared to those in industrial and residential combustion. There was a clear decline in traffic emissions in Beijing after the Spring Festival. As an immigrant city, a lot of people would leave Beijing to go back to their hometowns for the festival, which might cause a rapid decrease in traffic emissions.

The effects of the Spring Festival had been identified by the dynamic updates in Langfang, where the industrial emissions started to decrease about 3 days before the Spring Festival. The quality indicators were between medium and high for the rescaling factors in Langfang during the period of the Spring Festival. The changes in the emissions in Zhangjiakou were not significant, with average rescaling factors of about 0.96 for residential combustion, 0.95 for industry, and 1.02 for traffic. However, the general quality of the rescaling results for Zhangjiakou was relatively low, so more observations should be collected to further determine the emissions in the region.

The dynamically updated emissions in other regions were shown in Figs. S11 to S40 in the Supporting Information (SI). The emissions in some areas remained almost unchanged after the updates with low quality indicators, especially for those far from Beijing. It was mainly due to the limited transport of the pollutants from the corresponding regions to the measurement site. The weak signal detected by the measurements was too low to change the a priori emission based on the Bayesian Inference. The observations in this study were from a single site in Beijing. Multiple measurement sites with extensive spatial coverage could improve the ability to detect the contributions from various regions and thus the effectiveness of emission updates.

The temporal contributions of the primary $PM_{2.5}$ estimated by the atmospheric transport model with the updated emissions had good agreements with the results of the receptor model for residential combustion (Fig. 6(a)), traffic (Fig. 6(d)), and industrial sources (Fig. 6(g)). The statistical performance metrics, correlation coefficient (r), mean fractional bias (MFB), and mean fractional error (MFE), were calculated for the comparisons. For the residential combustion, the correlation coefficient between the source model and receptor model was significantly improved from 0.46 with the baseline emissions to 0.81 with the updated emissions, as shown in Fig. 6(b) and (c). The errors were also substantially reduced due to the updates of the emissions, from 1.16 to 0.16 for MFB and from 1.19 to 0.57 for MFE. The quantifications of the improved agreement between the source-oriented model and the receptor model due to the updates of emissions were also clearly shown in Fig. 6(e) and (f) for traffic and Fig. 6(h) and (i) for industrial sources.

3.5. Harmonized source apportionment

Fig. 7(a) shows the source apportionment results of the three different methods, i.e. the receptor model, the source-oriented model with the baseline emissions, and the harmonization of the models with the updated emissions. Both the uncertainties of the receptor model and the source-oriented model were taken into account with the L-curve method (Hansen, 2001) by assuming a balance between them as discussed in Section 3.3. As a result, the harmonization results in Fig. 7 were different from either the results of the receptor model or those of the source-oriented model. Since the results were achieved by the assumption of a balance of uncertainties in the two methods, the approach was called 'harmonization'.

All the results suggested that residential combustion was the dominant contributor to the primary $PM_{2.5}$ concentrations in Beijing during the investigated period. The harmonization of the receptor model and the source-oriented model utilized the information from both methods, and it indicated that the contributions of the primary $PM_{2.5}$ from residential combustion, traffic, and industry were about 60 %, 23 %, and 17 %, respectively.

The harmonized source apportionment in this study was compared with the previous studies for Beijing in the literature during the past two decades, as shown in Fig. 7(b). The contributions from the three major sectors to the primary $PM_{2.5}$ in Beijing were relatively stable between 2000 and 2012, as indicated by the long-term study (Wang et al., 2008) and the systematic review of the studies conducted between 2000 and 2012 (Lv et al., 2016), with industrial emission as the largest contributor. The annual

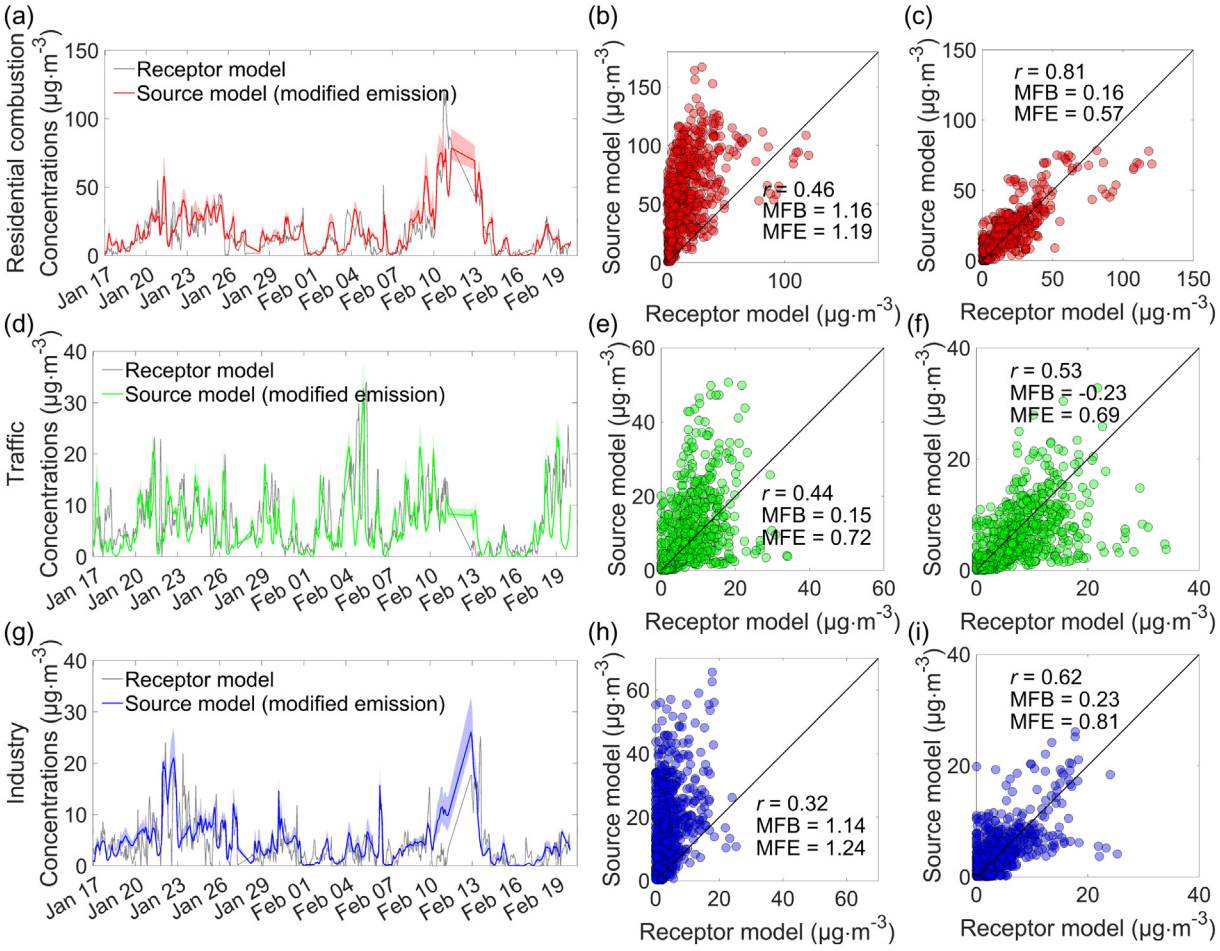

Fig. 6. Comparisons of the temporal contributions of primary $PM_{2.5}$ between the receptor model and the source-oriented model with the updated emissions from (a) residential combustion, (d) traffic and (g) industrial sources. The shaded areas indicated the maximum and minimum values corresponding to the feasible range of $\lambda_{receptor}/\lambda_{emission}$. The performance of the source-oriented with the baseline emissions (b), (e), (h) and with the updated emissions (c), (f), (i) from the three types of sources.

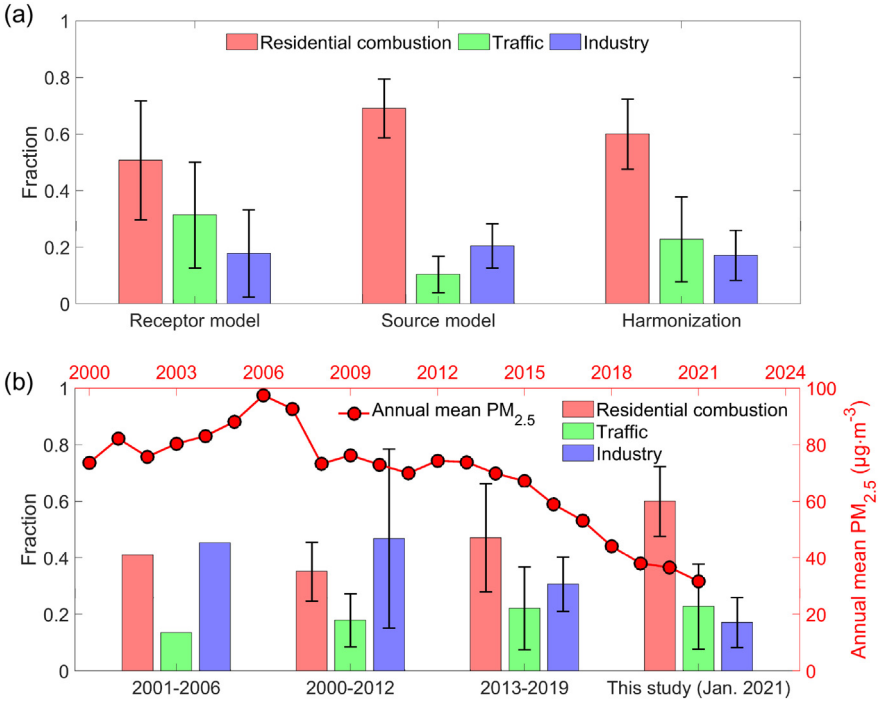

Fig. 7. Results of the source apportionment in Beijing. (a) The results of the receptor model, the source-oriented model with the baseline emissions, and the harmonization of the models with the updated emissions. The error bars show the standard deviations within the period of measurements. (b) Comparison with the source apportionment studies in Beijing in the literature for the last 20 years, including the long-term study between 2001 and 2006 (Wang et al., 2008), the systematic review of the studies conducted from 2000 to 2012 in Beijing (Lv et al., 2016), and the summary of the 13 recent studies between 2013 and 2019, and the details of the studies are shown in Table S2. The annual mean $PM_{2.5}$ concentrations in Beijing between 2000 and 2021 were available from the Tracking Air Pollution in China (TAP) database (Geng et al., 2021; Xiao et al., 2022) (http://tapdata.org.cn).

average $PM_{2.5}$ concentrations were also at high levels, about 80 μg m^{-3} during the same period. The $PM_{2.5}$ concentrations have continued to decline since 2013. The mitigation of the air pollution in Beijing has been achieved by the continuously decreasing contributions from industrial emissions, as indicated by the 13 recent studies between 2013 and 2019 (Chang et al., 2019; Gao et al., 2018; Guo et al., 2021; Hu et al., 2015; Huang et al., 2021; Liu et al., 2022; Liu et al., 2019; Ma et al., 2017; Park et al., 2022; Shi et al., 2017; Srivastava et al., 2021; Wen et al., 2021; Yang et al., 2016). The details of the 13 studies are shown in Table S2. The harmonized results in this study manifested the same trend with a lower contribution from the industry. It is important to note that the current study was for the heating period in winter, so the intensive contribution of residential combustion may deviate from the results for average annual conditions.

3.6. Regional contributions

Besides the source-specific contributions, which are available from the source apportionment results of receptor models, the source-oriented and the harmonized models also provided additional information about the regional contributions to the measurements. The major contributions of different regions to the source-specific primary $PM_{2.5}$ concentrations at the measurement site were shown in Fig. 8. The source-oriented model with the baseline emission for the year 2017 suggested that the local emissions in Beijing significantly contributed to the pollution (the red bars in Fig. 8). The high local contribution is consistent with the previous study using the CMAQ-ISAM source-oriented model (Chang et al., 2019), which found that the local emissions in Beijing contributed about 79 %, 72 %, and 79 % to the $PM_{2.5}$ from residential combustion, industry, and traffic in January 2014, respectively. A recent study has also revealed that the average local contribution to $PM_{2.5}$ in Beijing was about 65.6 % from 2001 to 2015 (Chen et al., 2021). However, the annual average $PM_{2.5}$ concentrations have constantly decreased since 2015, as shown in Fig. 7 (b), indicating the local contribution might have significantly changed during the past several years.

In the harmonized results using the updated emissions (the green bars in Fig. 8), the contributions of the local emissions in Beijing to the primary concentrations were substantially reduced compared with the results of the source-oriented model with the baseline emissions. According to the results of the source-oriented model using the baseline emissions, the local emissions in Beijing accounted for about 75 % of the primary $PM_{2.5}$ concentrations induced by residential combustion, but the share was significantly reduced to about 33 % using the updated emissions after the harmonization. The contributions from surrounding regions were notably increased. The contributions from Zhangjiakou increased from about 3 % to about 13 %, and the contributions from Langfang increased from about 5 % to about 11 %. Most of the primary $PM_{2.5}$ attributable to residential combustion (67 %) at the measurement site in Beijing was through transboundary transport. The local contribution to the primary $PM_{2.5}$ of traffic was slightly reduced from 81 % to 71 % after the harmonization (Fig. 8(b)), but contributions from the local industrial sources in Beijing were strongly reduced from 68 % to 17 % (Fig. 8(c)). A recent study (Dong et al., 2020) has observed the decreasing trend of the local contribution to $PM_{2.5}$ in Beijing, from about 61 % in 2014 to about 53 % in 2017. Another study (Chen et al., 2022) has also found that the average local contribution to $PM_{2.5}$ in Beijing was about 55 % between 2010 and 2019, significantly lower than the value between 2001 and 2015 (65.6 %) (Chen et al., 2021).

The shift of the regional contributions could be induced by both long-term and temporary reasons. First, the local management in Beijing had been strengthened during the past years to control the air pollution, e.g. the “coal-to-gas” transition, which could practically reduce the emission. The substantial reduction in the local contribution to the $PM_{2.5}$ of residential combustion might be mainly caused by the long-term effects. The temporary effects due to the special time periods, e.g. the Spring Festival

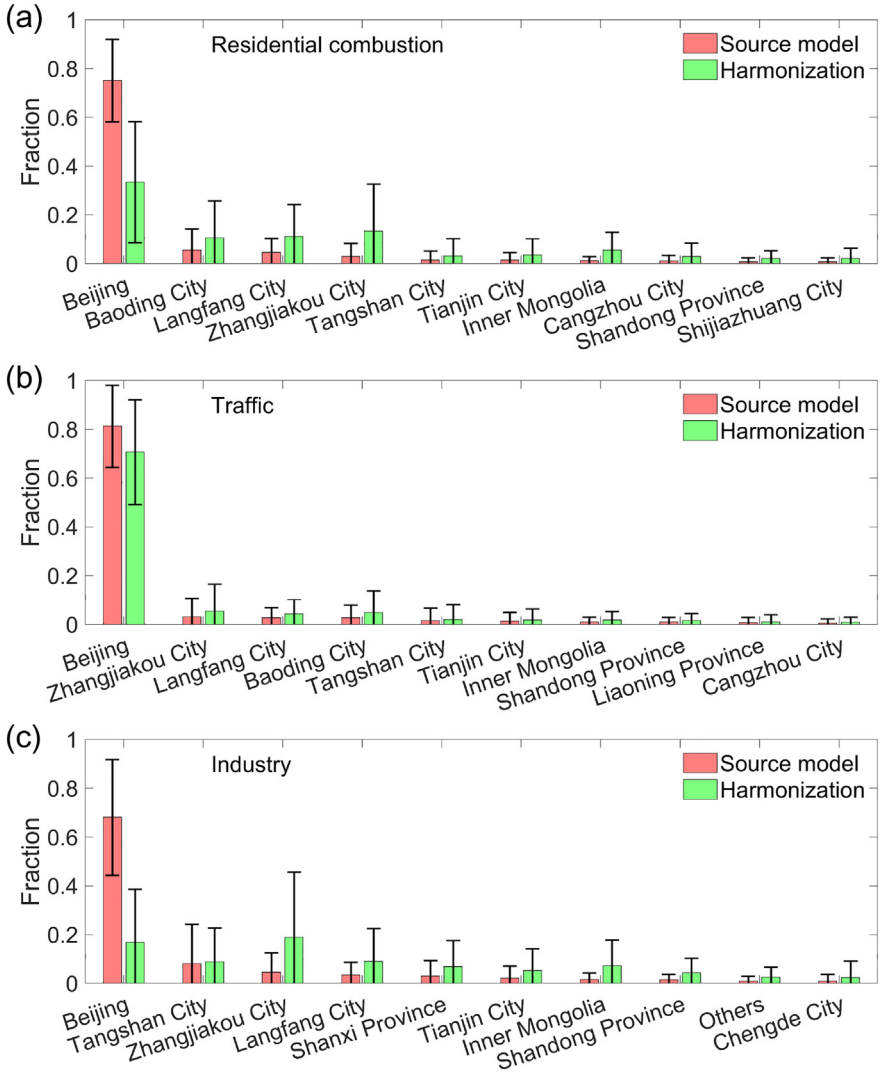

Fig. 8. Changes of the regional contributions with the baseline emissions and the harmonized updated emissions for (a) residential combustion, (b) traffic, and (c) industrial sources at the receptor site. The error bars were the standard deviations within the period of measurements.

and the COVID-19 pandemic (Feng et al., 2021), could also change the regional contributions.

It should be noted that the ability to distinguish the influences of different regions depends on the severity of the collinearity of their contributions to the observation site. The collinearity is quantified by the condition number of the sensitivity matrix. For the regions with the quality indicators of 'high', namely the dominant contributors with 90 % contributions to the measurements as introduced in Section 2.7, the condition numbers were usually below 100 as shown in Fig. S6(a), indicating no serious problem with collinearity (Montgomery et al., 2013). Fig. S7 shows a typical correlation matrix on Jan. 26 of the contributions from the regions with high quality. There was no significant correlation among these regions. The problem was well-conditioned. Physically speaking, the plumes from these dominant regions were not mixed together yet, so the influences could be numerically separated. As a result, the majority of the contributions (90 %) can be successfully attributed to these regions.

The condition numbers increased and the collinearity problem appeared around Feb. 15 as shown in Fig. S6(a). Relatively high correlations can be also identified in Fig. S8, which were mainly caused by the favorable dispersion conditions within the period. The wind speed and eddy diffusivity were high during this period (Fig. S9), leading to the rapid dispersion and mixing of the plumes from different regions. As a result, it became difficult to distinguish their influences. However, the time period with high condition numbers was short and the concentrations were low (Fig. 3) due to the favorable dispersion conditions, so it had limited effects considering the low contributions.

The condition numbers increased and became much higher than 100 as shown in Fig. S6(b), when the regions with medium quality were included, indicating moderate to strong collinearity problems (Montgomery et al., 2013). The condition numbers will further increase if the regions with low quality are included. As a result, regarding the remaining 10 % of the contributions of the regions with the quality indicators between medium and low, the plumes were relatively well mixed together due to the long transport distance. It became difficult to accurately distinguish the influences of the regions with medium to low quality. However, the remaining 10 % of the contribution should have limited effects on the major contributors.

Fig. 9 shows the temporal evolution of the contributions of the local emissions in Beijing and the emissions from the nearby city, Langfang. The results indicated that the reductions in the local contributions to the pollution of residential combustion (Fig. 9(a)) and industrial emissions (Fig. 9(c)) were relatively consistent within the whole investigated period, suggesting that the long-term effects might play an important role. However, the reductions in the local contributions to the traffic pollution (Fig. 9(b)) mainly happened in February near the Spring Festival (February 12), indicating that the short-term temporary effects might be the dominant

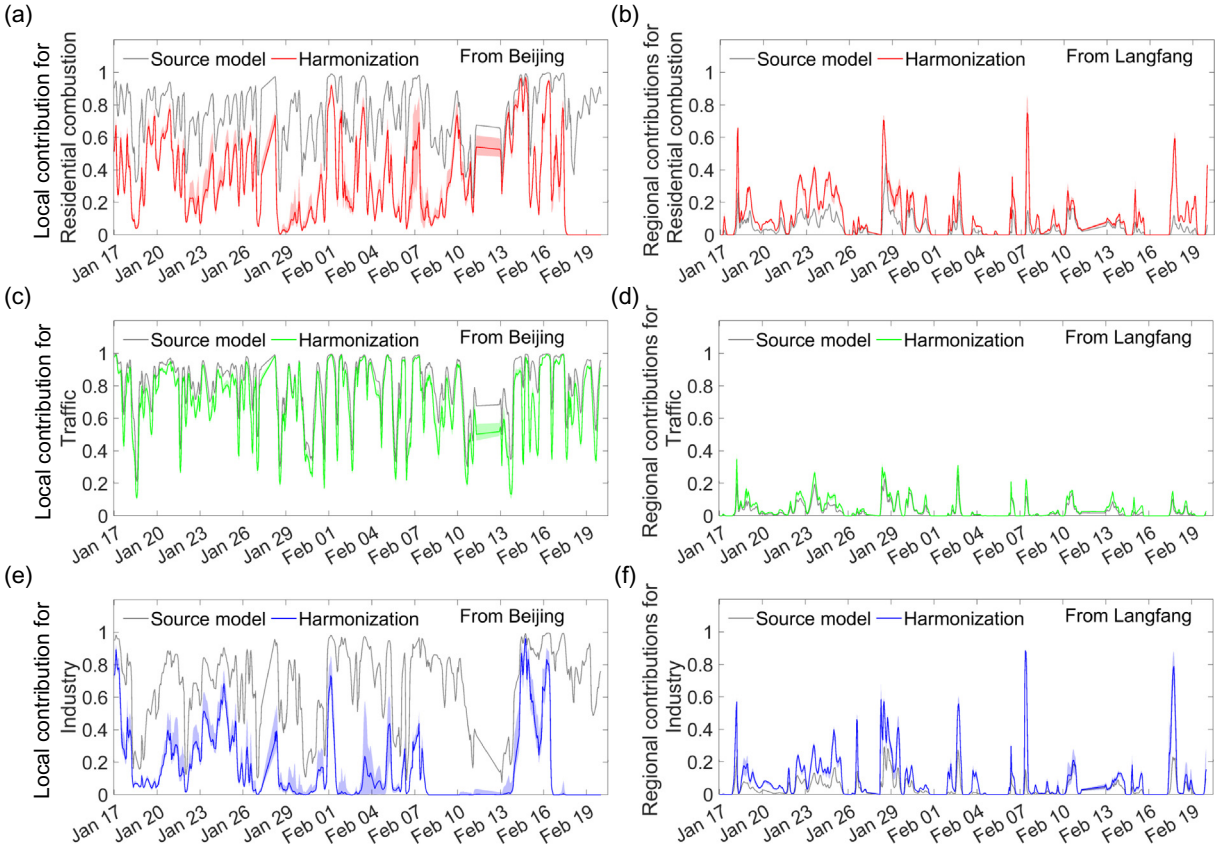

Fig. 9. Temporal evolution of the contributions of the primary $PM_{2.5}$ emissions in Beijing and Langfang to the measurements for (a) and (b) residential combustion, (c) and (d) traffic, and (e) and (f) for industrial sources.

reason. The contributions from nearby regions, e.g. Langfang, were increased, as shown in Fig. 9 (b), (d), and (f). As shown in Fig. 10, the local emissions in Beijing were the largest single contributor to the primary $PM_{2.5}$ from residential combustion (Fig. 10(a)) and traffic (Fig. 10(b)), but Zhangjiakou, in the northwest of Beijing, became the largest contributor to the primary $PM_{2.5}$ from industrial emissions (Fig. 10(c)) during the investigated period. The previous study also found that the regional transports were mainly from Zhangjiakou in January (Chang et al., 2019). In general, the dynamic updates of the emissions by the harmonization of the receptor model and the source-oriented model could successfully identify the changes in the emissions from the major types of sources and regional contributions.

4. Conclusions

In the current study, we have developed new methods to dynamically update the emission inventory by the combination of the source-oriented and receptor source apportionment models based on the Bayesian Inference. The combined method has been applied to a measurement campaign in Beijing from January to February 2021. The emissions of the three major types of anthropogenic sources, i.e. residential combustion, traffic, and industry, were hourly updated for 33 regions, and the impacts of the Spring Festival on the emissions have been successfully identified.

The results indicated that the local emission of primary $PM_{2.5}$ from residential combustion and industry in Beijing had significantly decreased by about 90 % during the investigated period compared with the baseline emission inventory from 2017. The primary emissions from traffic sources also had substantial decreases during the holidays of the Spring Festival, with an overall reduction of about 50 % during the investigated period compared to the baseline emission. The results suggested the reductions in emissions can be attributed to the long-term effects due to the three-year action plan to fight air pollution (2018–2020) and the "coal-to-gas" transition, and the short-term effects of the Spring Festival. The methods could be a promising pathway for the harmonization of source-oriented and receptor source apportionment models.

It should be noted that the data from a single measurement site in Beijing were utilized in the current study. The measurements could constantly detect the contributions from the local emissions in Beijing, but it might fail to receive the signals from other regions, especially the regions far away from the measurement site due to the variation of the wind field. More measurement sites with extensive spatial coverage are required in future studies to constantly detect the contributions from all the regions. The main purpose of this study was to harmonize the source-oriented and receptor source apportionment models and to update the primary $PM_{2.5}$ emissions, so only the primary $PM_{2.5}$ was investigated. The contributions of different sources might change if secondary aerosols are attributed to different sources based on the emitted precursors. The harmonization results were achieved by the assumption of a balance of uncertainties in the source-oriented and receptor methods using the L-curve method. The harmonization results can be further improved with a comprehensive quantification of the uncertainties in both methods, but it would be difficult considering that the emission inventory is not directly measurable and the receptor model is site-dependent.

CRediT authorship contribution statement

Xiaole Zhang: Conceptualization, Methodology, Investigation, Software, Data curation, Formal analysis, Visualization, Writing – original draft. **Xiaoxiao Feng:** Methodology, Software, Writing – review & editing.

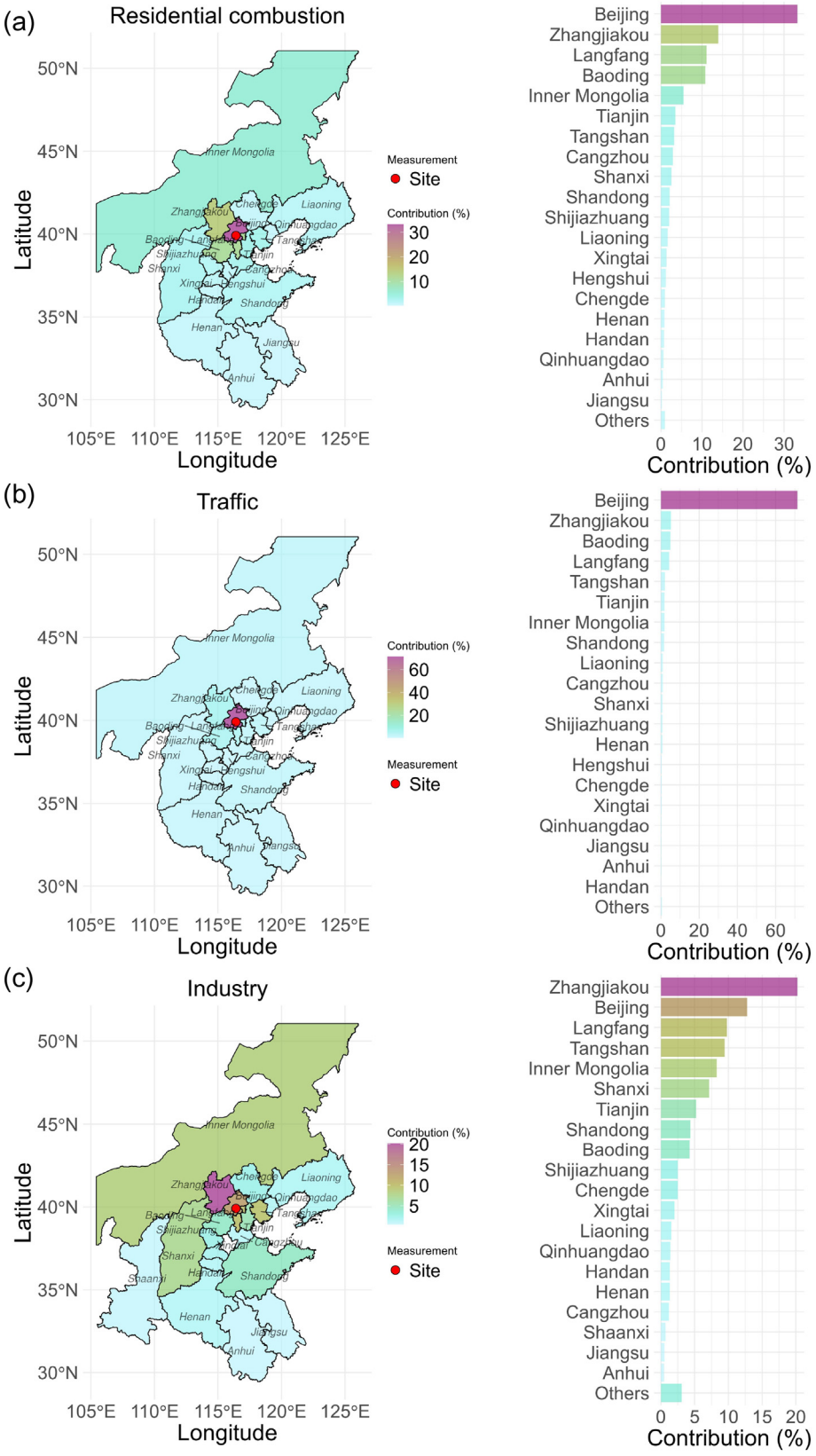

Fig. 10. Harmonization results for regional contributions to primary $PM_{2.5}$ concentrations at the measurement site due to the (a) residential combustion, (b) traffic, and (c) industrial sources.

Jie Tian: Software, Formal analysis, Investigation, Resources. **Yong Zhang:** Investigation, Data curation. **Zhiyu Li:** Investigation, Data curation. **Qiyuan Wang:** Resources, Supervision, Writing – review & editing. **Junji Cao:** Resources, Supervision, Project administration, Funding acquisition. **Jing Wang:** Conceptualization, Methodology, Resources, Writing – review & editing, Supervision, Project administration, Funding acquisition.

Data availability

Data will be made available on request.

Declaration of competing interest

The authors declare that they have no known competing financial interests or personal relationships that could have appeared to influence the work reported in this paper.

Acknowledgements

This study was supported by the project Clean Air China sponsored by Swiss Agency for Development and Cooperation, and the Youth Innovation Promotion Association of the Chinese Academy of Sciences (2022416).

Appendix A. Supplementary data

Supplementary data to this article can be found online at https://doi.org/10.1016/j.scitotenv.2022.160312.

References

Andronache, C., 2003. Estimated variability of below-cloud aerosol removal by rainfall for observed aerosol size distributions. Atmos. Chem. Phys. 3, 131–143.
Belis, C.A., Karagulian, F., Larsen, B.R., Hopke, P.K., 2013. Critical review and meta-analysis of ambient particulate matter source apportionment using receptor models in Europe. Atmos. Environ. 69, 94–108.
Cai, J.T., Wu, J.S., Yuan, S.Q., Kong, D.S., Zhang, X.L., 2022. Prediction of gas leakage and dispersion in utility tunnels based on CFD-EnKF coupling model: a 3D full-scale application. Sustain. Cities Soc. 80.
Chang, X., Wang, S., Zhao, B., Xing, J., Liu, X., Wei, L., et al., 2019. Contributions of inter-city and regional transport to PM2.5 concentrations in the Beijing-Tianjin-Hebei region and its implications on regional joint air pollution control. Sci. Total Environ. 660, 1191–1200.
Chen Antony, L.W., Cao, J., 2018. PM2.5 source apportionment using a hybrid environmental receptor model. Environ.Sci.Technol. 52, 6357–6369.
Chen, D., Liu, X., Lang, J., Zhou, Y., Wei, L., Wang, X., et al., 2017. Estimating the contribution of regional transport to PM2.5 air pollution in a rural area on the North China Plain. Sci. Total Environ. 583, 280–291.
Chen, D., Xia, L., Guo, X., Lang, J., Zhou, Y., Wei, L., et al., 2021. Impact of inter-annual meteorological variation from 2001 to 2015 on the contribution of regional transport to PM2.5 in Beijing, China. Atmos. Environ. 260, 118545.
Chen, D., Jin, X., Fu, X., Xia, L., Guo, X., Lang, J., et al., 2022. Impact of inter-annual variation in meteorology from 2010 to 2019 on the inter-city transport of PM2.5 in the Beijing–Tianjin–Hebei Region. Sustainability 14.
Crippa, M., Oreggioni, G., Guizzardi, D., Muntean, M., Schaaf, E., Lo Vullo, E., et al., 2019. Fossil CO2 and GHG Emissions of All World Countries - 2019 Report. EUR 29849 EN, ISBN 978-92-76-11100-9. Publications Office of the European Union, Luxembourg.
Crippa, M., Solazzo, E., Huang, G., Guizzardi, D., Koffi, E., Muntean, M., et al., 2020. High resolution temporal profiles in the Emissions Database for Global Atmospheric Research. Sci. Data 7, 121.
Dong, Z., Wang, S., Xing, J., Chang, X., Ding, D., Zheng, H., 2020. Regional transport in Beijing-Tianjin-Hebei region and its changes during 2014–2017: the impacts of meteorology and emission reduction. Sci. Total Environ. 737, 139792.
Feng, X., Zhang, X., He, C., Wang, J., 2021. Contributions of traffic and industrial emission reductions to the air quality improvement after the lockdown of Wuhan and neighboring cities due to COVID-19. Toxics 9, 358.
Forouzanfar, M.H., Afshin, A., Alexander, L.T., Anderson, H.R., Bhutta, Z.A., Biryukov, S., et al., 2016. Global, regional, and national comparative risk assessment of 79 behavioural, environmental and occupational, and metabolic risks or clusters of risks, 1990–2015: a systematic analysis for the Global Burden of Disease Study 2015. Lancet 388, 1659–1724.
Gao, J., Wang, K., Wang, Y., Liu, S., Zhu, C., Hao, J., et al., 2018. Temporal-spatial characteristics and source apportionment of PM2.5 as well as its associated chemical species in the Beijing-Tianjin-Hebei region of China. Environ. Pollut. 233, 714–724.
Gao, M., Zhang, X., Yue, Y., Qiu, T., Wang, J., Wang, X., 2022. Air path of antimicrobial resistance related genes from layer farms: emission inventory, atmospheric transport, and human exposure. J. Hazard. Mater. 430, 128417.
Gaydos, T.M., Pinder, R., Koo, B., Fahey, K.M., Yarwood, G., Pandis, S.N., 2007. Development and application of a three-dimensional aerosol chemical transport model,PMCAMx. Atmos. Environ. 41, 2594–2611.
Geng, G., Xiao, Q., Liu, S., Liu, X., Cheng, J., Zheng, Y., et al., 2021. Tracking air pollution in China: near real-time PM2.5 retrievals from multisource data fusion. Environ.Sci.Technol. 55, 12106–12115.
Guo, L.F., Chen, B.Z., Zhang, H.F., Fang, J.C., 2021. Prediction and source contribution analysis of PM2.5 using a combined FLEXPART model and Bayesian method over the Beijing-Tianjin-Hebei Region in China. Atmosphere 12.
Hansen, P.C., 2001. The L-curve and its use in the numerical treatment of inverse problems. Computational Inverse Problems in Electrocardiology. 4, pp. 119–142.
Henry, R.C., Lewis, C.W., Hopke, P.K., Williamson, H.J., 1984. Review of receptor model fundamentals. Atmos. Environ. (1967) 18 (18), 1507–1515.
Henze, D.K., Seinfeld, J.H., Shindell, D.T., 2009. Inverse modeling and mapping US air quality influences of inorganic PM2.5 precursor emissions using the adjoint of GEOS-Chem. Atmos. Chem. Phys. 9, 5877–5903.
Hopke, P.K., Ito, K., Mar, T., Christensen, W.F., Eatough, D.J., Henry, R.C., et al., 2006. PM source apportionment and health effects: 1. Intercomparison of source apportionment results. J. Expo. Sci. Environ. Epidemiol. 16, 275–286.
Hu, J., Wu, L., Zheng, B., Zhang, Q., He, K., Chang, Q., et al., 2015. Source contributions and regional transport of primary particulate matter in China. Environ. Pollut. 207, 31–42.
Hu, Y., Odman, M.T., Russell, A.G., 2009. Top-down analysis of the elemental carbon emissions inventory in the United States by inverse modeling using Community Multiscale Air Quality model with decoupled direct method (CMAQ-DDM). J. Geophys. Res. Atmos. 114.
Hu, Y., Balachandran, S., Pachon, J.E., Baek, J., Ivey, C., Holmes, H., et al., 2014. Fine particulate matter source apportionment using a hybrid chemical transport and receptor model approach. Atmos. Chem. Phys. 14, 5415–5431.
Huang, R.J., Zhang, Y.L., Bozzetti, C., Ho, K.F., Cao, J.J., Han, Y.M., et al., 2014. High secondary aerosol contribution to particulate pollution during haze events in China. Nature 514, 218–222.
Huang, X., Tang, G., Zhang, J., Liu, B., Liu, C., Zhang, J., et al., 2021. Characteristics of PM2.5 pollution in Beijing after the improvement of air quality. J. Environ. Sci. 100, 1–10.
Issartel, J.P., 2003. Rebuilding sources of linear tracers after atmospheric concentration measurements. Atmos. Chem. Phys. 3, 2111–2125.
Ivey, C.E., Holmes, H.A., Hu, Y.T., Mulholland, J.A., Russell, A.G., 2015. Development of PM2.5 source impact spatial fields using a hybrid source apportionment air quality model. Geosci. Model Dev. 8, 2153–2165.
Kalnay, E., 2003. Atmospheric Modeling, Data Assimilation and Predictability. Cambridge University Press.
Karagulian, F., Belis, C.A., Dora, C.F.C., Prüss-Ustün, A.M., Bonjour, S., Adair-Rohani, H., et al., 2015. Contributions to cities' ambient particulate matter (PM): a systematic review of local source contributions at global level. Atmos. Environ. 120, 475–483.
Karl, M., Pirjola, L., Grönholm, T., Kurppa, M., Anand, S., Zhang, X., et al., 2022. Description and evaluation of the community aerosol dynamics model MAFOR v2.0. Geosci. Model Dev. 15, 3969–4026.
Kelly, J.T., Baker, K.R., Nolte, C.G., Napelenok, S.L., Keene, W.C., Pszenny, A.A.P., 2016. Simulating the phase partitioning of NH3, HNO3, and HCl with size-resolved particles over northern Colorado in winter. Atmos. Environ. 131, 67–77.
Krysta, M., Bocquet, M., Brandt, J., 2008. Probing ETEX-II data set with inverse modelling. Atmos. Chem. Phys. 8, 3963–3971.
Kwok, R.H.F., Napelenok, S.L., Baker, K.R., 2013. Implementation and evaluation of PM2.5 source contribution analysis in a photochemical model. Atmos. Environ. 80, 398–407.
Lang, J., Cheng, S., Wen, W., Liu, C., Wang, G., 2017. Development and application of a new PM2.5 source apportionment approach. Aerosol Air Qual. Res. 17, 340–350.
Lang, J., Zhou, Y., Chen, D., Xing, X., Wei, L., Wang, X., et al., 2017. Investigating the contribution of shipping emissions to atmospheric PM2.5 using a combined source apportionment approach. Environ. Pollut. 229, 557–566.
Laupsa, H., Slordal, L.H., 2003. Applying model calculations to estimate urban air quality with respect to the requirements of the EU directives on NO2, PM10 and C6H6. Int. J. Environ. Pollut. 20, 309–320.
Laupsa, H., Denby, B., Larssen, S., Schaug, J., 2009. Source apportionment of particulate matter (PM2.5) in an urban area using dispersion, receptor and inverse modelling. Atmos. Environ. 43, 4733–4744.
Lelieveld, J., Evans, J.S., Fnais, M., Giannadaki, D., Pozzer, A., 2015. The contribution of outdoor air pollution sources to premature mortality on a global scale. Nature 525, 367.
Li, M., Liu, H., Geng, G., Hong, C., Liu, F., Song, Y., et al., 2017a. Anthropogenic emission inventories in China: a review. Natl. Sci. Rev. 4, 834–866.
Li, M., Zhang, Q., Kurokawa, J.I., Woo, J.H., He, K., Lu, Z., et al., 2017b. MIX: a mosaic Asian anthropogenic emission inventory under the international collaboration framework of the MICS-Asia and HTAP. Atmos. Chem. Phys. 17, 935–963.
Liu, L., Zhang, L., Wen, W., Jiao, J., Cheng, H., Ma, X., et al., 2022. Chemical composition, oxidative potential and identifying the sources of outdoor PM2.5 after the improvement of air quality in Beijing. Environ. Geochem. Health 2022, 1–17.
Liu, Y., Zheng, M., Yu, M., Cai, X., Du, H., Li, J., et al., 2019. High-time-resolution source apportionment of PM2.5 in Beijing with multiple models. Atmos. Chem. Phys. 19, 6595–6609.
Louis, J.-F., 1979. A parametric model of vertical eddy fluxes in the atmosphere. Bound.-Layer Meteorol. 17, 187–202.
Lv, B., Zhang, B., Bai, Y., 2016. A systematic analysis of PM2.5 in Beijing and its sources from 2000 to 2012. Atmos. Environ. 124, 98–108.
Ma, Q., Wu, Y., Tao, J., Xia, Y., Liu, X., Zhang, D., et al., 2017. Variations of chemical composition and source apportionment of PM2.5 during winter haze episodes in Beijing. Aerosol Air Qual. Res. 17, 2791–2803.
Mallet, V., Quélo, D., Sportisse, B., Ahmed de Biasi, M., Debry, É., Korsakissok, I., et al., 2007. Technical note: the air quality modeling system Polyphemus. Atmos. Chem. Phys. 7, 5479–5487.
Mircea, M., Calori, G., Pirovano, G., Belis, C.A., 2020. European guide on air pollution source apportionment for particulate matter with source oriented models and their combined use with receptor models. JRC Technical Report. Joint Research Centre (JRC), 21027 Ispra (VA), Italy.
Montgomery, D.C., Peck, E.A., Vining, G.G., 2013. Introduction to Linear Regression Analysis. Wiley.
Paatero, P., Tapper, U., 1994. POSITIVE MATRIX FACTORIZATION - A NONNEGATIVE FACTOR MODEL WITH OPTIMAL UTILIZATION OF ERROR-ESTIMATES OF DATA VALUES. Environmetrics 5, 111–126.

Park, J., Kim, H., Kim, Y., Heo, J., Kim, S.-W., Jeon, K., et al., 2022. Source apportionment of PM2.5 in Seoul, South Korea and Beijing, China using dispersion normalized PMF. Sci. Total Environ. 833, 155056.
Peng, L., Zhang, Q., Yao, Z., Mauzerall, D.L., Kang, S., Du, Z., et al., 2019. Underreported coal in statistics: a survey-based solid fuel consumption and emission inventory for the rural residential sector in China. Appl. Energy 235, 1169–1182.
Reff, A., Eberly, S.I., Bhave, P.V., 2007. Receptor modeling of ambient particulate matter data using positive matrix factorization: review of existing methods. J. Air Waste Manag. Assoc. 57, 146–154.
Shi, Z., Li, J., Huang, L., Wang, P., Wu, L., Ying, Q., et al., 2017. Source apportionment of fine particulate matter in China in 2013 using a source-oriented chemical transport model. Sci. Total Environ. 601–602, 1476–1487.
Skamarock, W.C., Klemp, J.B., Dudhia, J., Gill, D.O., Liu, Z., Berner, J., et al., 2019. A Description of the Advanced Research WRF Model Version 4. 145. National Center for Atmospheric Research, Boulder, CO, USA, p. 145.
Snoun, H., Bellakhal, G., Kanfoudi, H., Zhang, X., Chahed, J., 2019. One-way coupling of WRF with a Gaussian dispersion model: a focused fine-scale air pollution assessment on southern Mediterranean. Environ. Sci. Pollut. Res. 26, 22892–22906.
Srivastava, D., Xu, J., Vu, T.V., Liu, D., Li, L., Fu, P., et al., 2021. Insight into PM2.5 sources by applying positive matrix factorization (PMF) at urban and rural sites of Beijing. Atmos. Chem. Phys. 21, 14703–14724.
The-People's-Government-of-Beijing-Municipality, 2022. Beijing Energy Development Plan During the 14th Five-Year Plan Period (Date of Access: April 26, 2022), Beijing.
Thurston, G.D., Spengler, J.D., 1985. A QUANTITATIVE ASSESSMENT OF SOURCE CONTRIBUTIONS TO INHALABLE PARTICULATE MATTER POLLUTION IN METROPOLITAN BOSTON. Atmos. Environ. 19, 9–25.
Tian, J., Wang, Q., Liu, H., Ma, Y., Liu, S., Zhang, Y., et al., 2021a. Measurement report: the importance of biomass burning in light extinction and direct radiative effect of urban aerosol during the COVID-19 lockdown in China. Atmos. Chem. Phys. Discuss. 2021, 1–29.
Tian, J., Wang, Q., Zhang, Y., Yan, M., Liu, H., Zhang, N., et al., 2021b. Impacts of primary emissions and secondary aerosol formation on air pollution in an urban area of China during the COVID-19 lockdown. Environ. Int. 150, 106426.
Troen, I.B., Mahrt, L., 1986. A simple model of the atmospheric boundary layer; sensitivity to surface evaporation. Bound.-Layer Meteorol. 37, 129–148.
Uranishi, K., Ikemori, F., Nakatsubo, R., Shimadera, H., Kondo, A., Kikutani, Y., et al., 2017. Identification of biased sectors in emission data using a combination of chemical transport model and receptor model. Atmos. Environ. 166, 166–181.
Venkatram, A., Pleim, J., 1999. The electrical analogy does not apply to modeling dry deposition of particles. Atmos. Environ. 33, 3075–3076.
Viana, M., Querol, X., Alastuey, A., Gil, J.I., Menéndez, M., 2006. Identification of PM sources by principal component analysis (PCA) coupled with wind direction data. Chemosphere 65, 2411–2418.
Viana, M., Kuhlbusch, T.A.J., Querol, X., Alastuey, A., Harrison, R.M., Hopke, P.K., et al., 2008. Source apportionment of particulate matter in Europe: a review of methods and results. J. Aerosol Sci. 39, 827–849.
Wagstrom, K.M., Pandis, S.N., Yarwood, G., Wilson, G.M., Morris, R.E., 2008. Development and application of a computationally efficient particulate matter apportionment algorithm in a three-dimensional chemical transport model. Atmos. Environ. 42, 5650–5659.
Wang, H., Zhuang, Y., Wang, Y., Sun, Y., Yuan, H., Zhuang, G., et al., 2008. Long-term monitoring and source apportionment of PM2.5/PM10 in Beijing, China. J. Environ. Sci. 20, 1323–1327.
Wang, S., Su, H., Chen, C., Tao, W., Streets, D.G., Lu, Z., et al., 2020. Natural gas shortages during the "coal-to-gas" transition in China have caused a large redistribution of air pollution in winter 2017. Proc. Natl. Acad. Sci. 117, 31018–31025.
Wang, Y., Huang, H., Huang, L., Zhang, X., 2018. Source term estimation of hazardous material releases using hybrid genetic algorithm with composite cost functions. Eng. Appl. Artif. Intell. 75, 102–113.
Wang, Z.S., Chien, C.J., Tonnesen, G.S., 2009. Development of a tagged species source apportionment algorithm to characterize three-dimensional transport and transformation of precursors and secondary pollutants. J. Geophys. Res. Atmos. 114.
Watson, J.G., Cooper, J.A., Huntzicker, J.J., 1984. The effective variance weighting for least squares calculations applied to the mass balance receptor model. Atmos. Environ. (1967) 1984 (18), 1347–1355.
Wen, W., Shen, S., Liu, L., Ma, X., Wei, Y., Wang, J.K., et al., 2021. Comparative analysis of PM2.5 and O-3 source in Beijing using a chemical transport model. Remote Sens. 13.
Wu, J., Yuan, S., Zhang, C., Zhang, X., 2018. Numerical estimation of gas release and dispersion in coal mine using Ensemble Kalman Filter. J. Loss Prev. Process Ind. 56, 57–67.
Wu, J.S., Cai, J.T., Yuan, S.Q., Zhang, X.L., Reniers, G., 2021. CFD and EnKF coupling estimation of LNG leakage and dispersion. Saf. Sci. 139.
Xiao, Q., Geng, G., Liu, S., Liu, J., Meng, X., Zhang, Q., 2022. Spatiotemporal Continuous Estimates of Daily 1-km PM2.5 From 2000 to Present Under the Tracking Air Pollution in China (TAP) Framework.
Yang, H., Chen, J., Wen, J., Tian, H., Liu, X., 2016. Composition and sources of PM2.5 around the heating periods of 2013 and 2014 in Beijing: implications for efficient mitigation measures. Atmos. Environ. 124, 378–386.
Ying, Q., Feng, M., Song, D., Wu, L., Hu, J., Zhang, H., et al., 2018. Improve regional distribution and source apportionment of PM2.5 trace elements in China using inventory-observation constrained emission factors. Sci. Total Environ. 624, 355–365.
Yuan, S., Wu, J., Zhang, X., Liu, W., 2019. EnKF-based estimation of natural gas release and dispersion in an underground tunnel. J. Loss Prev. Process Ind. 62, 103931.
Zhang, C., Chen, L., Ding, S., Zhou, X., Chen, R., Zhang, X., et al., 2022a. Mitigation effects of alternative aviation fuels on non-volatile particulate matter emissions from aircraft gas turbine engines: a review. Sci. Total Environ. 153233.
Zhang, J., Zhang, S., Zhang, X., Wang, J., Wu, Y., Hao, J., 2022b. Developing a high-resolution emission inventory of China's aviation sector using real-world flight trajectory data. Environ.Sci.Technol. 56, 5743–5752.
Zhang, X., Huang, M., 2017. Ensemble-based release estimation for accidental river pollution with known source position. J. Hazard. Mater. 333, 99–108.
Zhang, X., Wang, J., 2021. Dose-response relation deduced for coronaviruses from coronavirus disease 2019, severe acute respiratory syndrome, and Middle East Respiratorysyndrome: meta-analysis results and its application for infection risk assessment of aerosol transmission. Clin. Infect. Dis. 73, e241–e245.
Zhang, X., Wang, J., 2022. Atmospheric dispersion of chemical, biological, and radiological hazardous pollutants: informing risk assessment for public safety. J.Saf.Sci.Resilience 3, 372–397.
Zhang, X., Raskob, W., Landman, C., Trybushnyi, D., Li, Y., 2017. Sequential multi-nuclide emission rate estimation method based on gamma dose rate measurement for nuclear emergency management. J. Hazard. Mater. 325, 288–300.
Zhang, X., Efthimiou, G., Wang, Y., Huang, M., 2018. Comparisons between a new point kernel-based scheme and the infinite plane source assumption method for radiation calculation of deposited airborne radionuclides from nuclear power plants. J. Environ. Radioact. 184–185, 32–45.
Zhang, X., Chen, X., Wang, J., 2019. A number-based inventory of size-resolved black carbon particle emissions by global civil aviation. Nat. Commun. 10, 534.
Zhang, X., Karl, M., Zhang, L., Wang, J., 2020. Influence of aviation emission on the particle number concentration near Zurich Airport. Environ.Sci.Technol. 54, 14161–14171.
Zhang, X., Ji, Z., Yue, Y., Liu, H., Wang, J., 2021. Infection risk assessment of COVID-19 through aerosol transmission: a case study of South China seafood market. Environ.Sci. Technol. 55, 4123–4133.
Zhang, X.L., Chen, J.G., Su, G.F., Yuan, H.Y., 2013. Study on source inversion technology for nuclear accidents based on Gaussian puff model and EnKF. In: Comes, T., Fiedrich, F., Fortier, S., Geldermann, J., Müller, T. (Eds.), 10th International Conference on Information Systems for Crisis Response and Management, Baden-Baden, Germany, pp. 634–639.
Zhang, X.L., Su, G.F., Yuan, H.Y., Chen, J.G., Huang, Q.Y., 2014. Modified ensemble Kalman filter for nuclear accident atmospheric dispersion: prediction improved and source estimated. J. Hazard. Mater. 280, 143–155.
Zhang, X.L., Li, Q.B., Su, G.F., Yuan, M.Q., 2015a. Ensemble-based simultaneous emission estimates and improved forecast of radioactive pollution from nuclear power plant accidents: application to ETEX tracer experiment. J. Environ. Radioact. 142, 78–86.
Zhang, X.L., Su, G.F., Chen, J.G., Raskob, W., Yuan, H.Y., Huang, Q.Y., 2015b. Iterative ensemble Kalman filter for atmospheric dispersion in nuclear accidents: an application to Kincaid tracer experiment. J. Hazard. Mater. 297, 329–339.
Zhang, Y., Wang, Q.Y., Tan, J., Li, Y., Liu, H.K., Ran, W.K., et al., 2022. High Time Resolution Measurements of PM2.5 in Northern Cities of China: Chemical Composition, Source Apportionment and Policy Implications (submitted for publication).
Zhao, S., Russell, M.G., Hakami, A., Capps, S.L., Turner, M.D., Henze, D.K., et al., 2020. A multiphase CMAQ version 5.0 adjoint. Geosci. Model Dev. 13, 2925–2944.
Zheng, B., Zhang, Q., Tong, D., Chen, C., Hong, C., Li, M., et al., 2017. Resolution dependence of uncertainties in gridded emission inventories: a case study in Hebei,China. Atmos. Chem. Phys. 17, 921–933.
Zheng, B., Tong, D., Li, M., Liu, F., Hong, C., Geng, G., et al., 2018. Trends in China's anthropogenic emissions since 2010 as the consequence of clean air actions. Atmos. Chem. Phys. 18, 14095–14111.
Zheng, B., Cheng, J., Geng, G., Wang, X., Li, M., Shi, Q., et al., 2021. Mapping anthropogenic emissions in China at 1 km spatial resolution and its application in air quality modeling. Sci.Bull. 66, 612–620.
Zhu, Y., Huang, L., Li, J., Ying, Q., Zhang, H., Liu, X., et al., 2018. Sources of particulate matter in China: insights from source apportionment studies published in 1987–2017. Environ. Int. 115, 343–357.